PARTICLE MASS TRANSFER COEFFICIENTS FOR COCURRENT GAS-LIQUID FLOW IN PACKED BEDS

by

Ching-Shi Yang

A thesis submitted in partial fulfillment of
the requirements for the degree of

Master of Applied Science

to the

School of Graduate Studies
University of Ottawa
Ottawa, Ontario, Canada.

May 1978.

ABSTRACT

Particle-liquid mass transfer coefficients were determined by measuring the rate of dissolution of benzoic acid into water in a packed bed column with downward cocurrent flows. The packing consisted of 6.35 mm Berl saddles coated with benzoic acid and fluorescent dye mixture. The water flow rate was varied between 2.1 and 98 kg/m^2 sec and the air flow rate between 0.33 and 1.77 kg/m^2 sec covering the gas continuous, transition, pulsing, and dispersed bubble flow regimes. The effect of the gas flow rate on the mass transfer coefficient is less important in the trickling and dispersed bubble flow regimes and becomes significant in the transition and pulsing flow regimes. Correlations in terms of modified Sherwood number and modified Reynolds number are presented.

ACKNOWLEDGEMENTS

The author would like to express his gratitude to Professor W. Hayduk for his advice, direction as thesis supervisor, without whose idea and patience this work could not have been carried out.

He also wishes to acknowledge Dr. J.A. Ruether for the help he provided at the early stages of this work.

Also, the author is indebted to Mr. G. Gasperetti and his assistants for their help in constructing the apparatus.

TABLE OF CONTENTS

LIST OF FIGURES

LIST OF TABLES

NOMENCLATURE

a_G	gas/liquid mass transfer interfacial area per unit volume, m^{-1}
a_S	liquid/solid mass transfer interfacial area per unit volume, m^{-1}
a_V	particle external area per unit volume of the test part, m^{-1}
a_W	wetted area per unit volume of the test part, m^{-1}
A_p	average particle surface area, m^2
A	surface area of mass transfer for solute on a particle, m^2
C_D	concentration of fluorescent dye leaving the column, g/l
C_i^*	concentration in gas phase at gas-liquid interphase, $mole/m^3$
C_i	concentration in liquid phase at gas-liquid interphase, $mole/m^3$
C_L	bulk concentration, $mole/m^3$
C_O	concentration of benzoic acid at inlet, g/l
C_1	concentration of benzoic acid at outlet, g/l
C_S	concentration at liquid/solid interface, $mole/m^3$, or solubility of benzoic acid, g/l
d_P	effective particle diameter, m
D	diffusivity of solute in the liquid, m^2/s
E_L	power dissipation by the liquid phase per unit volume of the bed, $(-\Delta P/Z)_{LG}.V_L$, W/m^3

E_L'	power dissipation by the liquid phase per unit mass of liquid holdup, $E_L/(h_L\rho_L)$, W/kg
Ga^*	modified Galileo number, dimensionless
g	acceleration of gravity, m/s^2
G	gas superficial mass flow rate, kg/m^2s
h_L	liquid total holdup, m^3 of liquid/m^3 of bed volume
h_{LD}	dynamic liquid holdup, m^3 of liquid/m^3 of bed volume
J_D	mass transfer factor, $(k_S\phi/V_L).(\mu_L/D\rho_L)^{2/3}$, dimensionless
k	specific catalytic rate constant, m/s
k_G	mass transfer coefficient for gas-phase film, m/s
k_L	mass transfer coefficient for liquid-phase film, m/s
k_S	mass transfer coefficient for liquid/solid, m/s
Ko	liquid phase Kolmogoroff number, $(E_L'd_P^4\rho_L^3/\mu_L^3)$, dimensionless
L	liquid superficial mass flow rate, kg/m^2s
n	number of particles in the test part
N	molal flux of solute, $mole/m^3s$
r	ratio of benzoic acid to fluorescent dye
R	reading of manometer, m
R_O	reading of manometer without flow, m
Re_G	gas Reynolds number, $(V_Gd_P\rho_G/\mu_G)$, dimensionless
Re_L	liquid Reynolds number, (Ld_P/μ_L), dimensionless
Re_L'	modified liquid Reynolds number, $(L/h_La_S\mu_L)$, dimensionless

Sc	Schmidt number, $(\mu_L/\rho_L D)$, dimensionless
Sh	Sherwood number, $(k_S d_P/D)$, dimensionless
Sh'	modified Sherwood number, $(k_S/a_S D)$, dimensionless
t	bulk temperature, °C
U_L	average actual liquid velocity, V_L/h_L, m/s
V_G	gas superficial velocity, m/s
V_L	liquid superficial velocity, m/s
Z	height of pack bed or vertical distance between taps, m
Z*	parameter, $Re_G^{1.167}/Re_L^{0.767}$, dimensionless
Z_B	height of test part, m

Greek letters

β_D	dynamic liquid saturation, dimensionless
β_S	static liquid saturation, dimensionless
ΔP	pressure drop; ΔP_L for single phase liquid flow, ΔP_G for single phase gas flow, ΔP_{LG} for mixed phase flow, kg/m^2s^2
Δm_B	weight of benzoic acid, kg
Δm_D	weight of fluorescent, kg
ε	void fraction in packed bed
μ_G	viscosity of gas phase, kg/ms
μ_L	viscosity of liquid phase, kg/ms
μ_W	viscosity of water, kg/ms
ρ	density of benzoic acid and fluorescent dye mixture, kg/m^3

ρ_B	density of benzoic acid, kg/m^3
ρ_D	density of fluorescent dye, kg/m^3
ρ_L	density of liquid phase, kg/m^3
ρ_W	density of water, kg/m^3
σ_L	liquid phase surface tension, kg/s^2
σ_W	surface tension of water, kg/s^2
ϕ	fractional wetted area, a_W/a_S, ϕ varies between 0 and 1
χ	Lockhart-Martinelli's parameter
η	intraparticle effectiveness
ψ	$(\sigma_W/\sigma_L)\ ((\mu_L/\mu_W)(\rho_W/\rho_L)^2)^{1/3}$, dimensionless

INTRODUCTION

In recent years, the cocurrent downward passage of liquid and gas through a packed column has been widely used in chemical industries either in absorption apparatuses or in catalytic reactors (trickle-bed reactors) in particular for such processes as the hydrodesulfurization or the hydrocracking of heavy oil stocks, the hydrotreating and refining of lubricating oil, the synthesis of butynediol, the production of sorbitol and the oxidation of organic pollutants (1,27).

In a trickle bed reactor, the reactants in the gas phase must be absorbed and be transported by liquid turbulence and diffusion to the catalyst surface and then through the liquid-filled pores to the interior sites to react with the reactants in the liquid phase. If the reaction is a first-order irreversible catalytic reaction, the steady-state flux equation may be expressed as:

$$N = k_G a_G (C_G - C_{iG}) \quad \text{(bulk gas to interface)}$$

$$= k_L a_G (C_{iL} - C_L) \quad \text{(interface to bulk liquid)}$$

$$= k_S a_S (C_L - C_S) \quad \text{(bulk liquid to catalyst surface)}$$

$$= \eta k a_S C_S \quad \text{(catalyst surface reaction)} \quad (1)$$

Therefore, there are four mass transfer resistances in a trickle bed reactor as $1/k_G a_G$, $1/k_L a_G$, $1/k_S a_S$ and $1/\eta k a_S$. The resistance at the gas-liquid interface, $1/k_G a_G$, can be neglected if the gas is relatively insoluble in, and in

equilibrium with the liquid phase.

For proper design of trickle bed reactors it is necessary to know the mass transfer coefficients between phases. This type of reactor has been widely investigated during the past decade and considerable information is available in the literature. However, information about liquid-particle mass transfer coefficients is meager.

The purpose of this study was to obtain mass transfer data over a moderate range of liquid rates by measuring the rate of dissolution of benzoic acid into water. Data obtained in the Reynolds number range (Re'_L) of 20 to 500 were correlated and compared with the published data.

HYDRODYNAMICS OF COCURRENT OPERATION

I. Flow Patterns

The flow patterns encountered in a trickle bed reactor play an important role in the mass transfer rate (13). Therefore, it is necessary to characterize the flow patterns before any mass transfer data are presented.

In recent years a number of publications have appeared that describe the flow patterns. The main articles are by Weekman et al. (4), Turpin et al. (22), Sato et al. (5), Charpentier et al. (25), and Talmor (18).

Weekman et al. (4) first classified these flow patterns into the gas continuous, transition and pulsing flow regimes. These were later reclassified by Sato et al. (5) as the gas continuous, transition, pulsing, and dispersed bubble flow regimes. Talmor (18) recently termed the flow patterns two continuous phases (channeled or trickling flow), gas continuous (spray or blurring flow), liquid continuous (dispersed bubble), pulsing and bubbling/pulsing flow regimes.

At a sufficiently low gas flow and liquid flow, trickling flow is encountered, where the flow of one phase is little affected by the flow of the other. Part of the packing is surrounded with a laminar liquid film and part is incompletely wetted. As the gas flow rate is increased, the liquid film become thinner and turbulent. Part of the liquid is carried as a mist in the gas stream. This patterns is called spray flow. As the gas flow rate is increased further, more and more

liquid is carried until nearly all of the liquid is entrained in the gas stream (22). If the liquid flow rate is increased further at a moderate gas flow rate, a nonhomogeneous flow regime, the transition flow, is encountered. Pulses may exist occasionally near the bottom of the packed bed. If the liquid flow rate is then increased, liquid and gas traverse the bed in the form of segregated slugs (pulses) which consist of alternate portions of more dense (liquid rich) and less dense (gas rich) mixtures of the two phases. This is termed pulsing flow regime. With a further increase in the liquid flow rate, the observed pulses are brought closer and closer together which eventually disappear owing to high shear stress at the gas-liquid interface. The gas disperses into bubbles flowing unbroken in the liquid continuous phase, producing the fourth flow pattern - dispersed bubble flow.

Fukushima et al. (21) and Talmor (18) have prepared flow maps which allow prediction of the state of flow from a knowledge of flow variables.

II. Pressure Drop

For a given gas and liquid flow rate in a trickle bed reactor, the pressure gradient changes gradually at the entrance region, reaching a constant value further down. Therefore, the end effect should be taken into consideration in measuring pressure drop.

Owing to the discontinuity of the phase distribution in the pulsing flow regime, the pressure suddenly increases

as the pulse front (liquid rich) passes through the measuring point, then decreases. A pressure oscillation is thus encountered. Fluctuations in pressure are greatest at the transition flow regime. As the liquid flow rate increases, the frequency of pressure oscillations is increased but the amplitude of fluctuations decreases.

While the local pressure drops for the various column sections were found to oscillate in correspondence with the passing pulses, Talmor (18) found that the overall pressure drop was steady but increasing, depending on the extent of the pulsing, and on liquid holdup in the bed. The increase in pressure drop due to pulsing is less in large size packing than in smaller size packing.

The Larkins (20), Sato (15) and Specchia (6) equations can be used to predict the pressure drop in a trickle bed reactor. Larkins and Sato adopted the Lockart and Martinelli (23) approach for cocurrent two-phase flow in pipes as shown in Equation 2 and 3, respectively.

$$\log \frac{\Delta p_{LG}}{\Delta p_L + \Delta p_G} = \frac{0.416}{(\log \chi)^2 + 0.666} \tag{2}$$

$$\log \frac{\Delta p_{LG}}{\Delta p_L + \Delta p_G} = \frac{0.70}{\log (\chi/1.2)^2 + 1.00} \tag{3}$$

Specchia correlated their data with an Ergun-type equation (24) as follows:

$$\Delta p_{LG} = k_1 \frac{\left(1-\varepsilon(1-\beta_S-\beta_D)\right)^2}{\varepsilon^3(1-\beta_S-\beta_D)^3} \mu_G V_G$$

$$+ k_2 \frac{1-\varepsilon(1-\beta_S-\beta_D)}{\varepsilon^3(1-\beta_S-\beta_D)^3} \rho_G V_G^2 \qquad (4)$$

In the above expression k_1 and k_2 are coefficients depending on packing shape and size.

III. Liquid Holdup

A knowledge of liquid holdup in the bed not only provides useful information concerning liquid residence times, and operating bed porosity, but also is very valuable in interpreting mass transfer results. Liquid holdup is generally expressed as the volume of liquid present per volume of empty reactor and can be divided into two parts (1) dynamic holdup (operating holdup), and (2) static holdup (residual holdup). Dynamic holdup is determined by suddenly stopping the liquid feed by a quick-closing electrical valve and collecting the draining liquid for a specified time, the recommended time being 15 minutes. Static holdup is the fraction of the liquid remaining in the packing after drainage. Dynamic holdup is a function of the gas and liquid flow rates, the characteristics of the packing, and the properties of the fluid. Static holdup is a function of the physical properties of the liquid phase. For a given liquid flow rate, it is observed that as the gas flow rate is increased, the dynamic holdup keeps nearly constant in trickling flow, decreases sharply in pulsing flow, and again decreases slightly in spray flow (25). Specchia et al. (14) found that when the gas flow rate was increased to a sufficiently high value, liquid holdup reached an asymptotic,

constant value.

Since the work of Larkins et al. (20), a large amount of liquid holdup data has been published (6,15,22,25, 26). Larkins et al. reported liquid holdup data including 3 mm glass spheres and 3 mm catalyst cylinders and correlated them in terms of the χ parameter as follows:

$$\log(h_L/\varepsilon) = -0.774 + 5.25 \log \chi - 0.109(\log \chi)^2 \qquad (5)$$

$$\text{for } 0.05<\chi<30$$

Sato et al. (15) presented their empirical equation for 16.5 mm to 25.9 mm glass spheres as evaluated with the χ parameter and a parameter a_S, that is

$$\log(h_L/\varepsilon) = 0.40\, a_S^{\,1/3}\, \chi^{\,0.22} \qquad (6)$$

$$\text{for } 0.1<\chi<20$$

Turpin's (22) total liquid holdup data for 7.62 mm and 8.23 mm tubular alumina particles were correlated in terms of the ratio of the mass flow rates of the respective phases. Charpentier et al. (25) obtained liquid holdup data for cylindrical particles by examining several foaming and nonfoaming systems and correlated these data in terms of the modified χ parameter as follows:

$$\log(h_L/\varepsilon) = -0.363 + 0.168 \log \chi' - 0.043 (\log \chi')^2 \qquad (7)$$

In the above expression χ' was defined as:

$$\chi' = \sqrt{\frac{\frac{L}{G}}{\frac{1}{\rho_G g_c} \cdot \frac{\Delta p_G}{Z} + 1}} \qquad (8)$$

Fukushima et al. (21) presented their data in terms of the gas and liquid Reynolds number, the surface shape factor of the packing, the void fraction and the ratio of packing size to column diameter. They found that the correlation equation for dispersed bubble flow is different from those for other flow regimes.

The most recent data show that dynamic and static holdup depend on different parameters (6,25), so that correlating dynamic holdup seems to yield more accurate results than correlating total holdup. Specchia et al. (6) proposed empirical correlations of dynamic holdup in spherical and cylindrical particles by postulating two hydrodynamic regimes: a poor (corresponding to gas continuous) and a high (corresponding to pulsing and spray flow) gas-liquid interaction regime as follows:

1. For poor interaction regime:

$$\beta_D = 3.86 \quad (Re_L)^{0.545} \; (Ga^*)^{-0.42} \left(\frac{a_S d_P}{\varepsilon} \right)^{0.65} \qquad (9)$$

2. For high interaction regime:

$$\beta_D = 0.125 \quad \left(Z^*/\psi^{1.1}\right)^{-0.312} \left(\frac{a_S d_p}{\varepsilon} \right)^{0.65} \qquad (10a)$$

for non-foaming system

$$\beta_D = 0.0616 \quad \left(Z^*/\psi^{1.1}\right)^{-0.172} \left(\frac{a_S d_p}{\varepsilon} \right)^{0.65} \qquad (10b)$$

for foaming system

According to their reports, the equations fit experimental results from several investigators(15,20,26) better than those proposed in the literature.

In this study, the flow patterns were determined by visual observation and were categoried into four flow regimes according to Sato's classification (5). It should be noted that there were no abrupt changes of flow pattern with gas or liquid flow rate. The pressure drop was measured directly by means of a manometer and was used to calculate the liquid dynamic holdup and power dissipation. Specchia's correlation equation (6) was used to determine dynamic holdup. Static holdup was assumed to be independent of varying gas and liquid flow rates as in the case of countercurrent operation (35). A value of static holdup was obtained two sources, the first obtained by measurement by Standish (36), who used 1/4 in. Berl saddles as the packing material and the second which was extrapolated by using the correlation of Shulman et al. (35) for Berl saddles. An average of the two,0.0803, and 0.0856, respectively, was used. A sample calculation for liquid holdup is list in Appendix IV.

THE FLUORESCENT-DYE TECHNIQUE

The fluorescent-dye technique used throughout this research was first used by Lemay et al. (3) and validated for use in mass transfer studies. In this method, the diffusion material was the dye-benzoic acid mixture. The rate of dissolution of the particles were measured by using a fluorometer. It is based on the principle that since the solubility of the dye is much greater than that of benzoic acid, the rate of release of the dye into a solution is controlled by the rate of dissolution of benzoic acid. Once the concentration of the dye is measured, the concentration of dissolved benzoic acid can be given immediately by means of the previously obtained ratio of the benzoic acid to the dye.

The advantages of a fluorescent-dye method of analysis as compared to a titration method have been discussed by Lemay et al. (3). Briefly, the sensitivity of the fluorometer allows it to measure a dye concentration as low as 10^{-8}g/l, corresponding to a benzoic acid concentration of 10^{-4} M if a solution containing a 99:1 weight ratio of benzoic acid to dye is measured. Another advantage is that the concentration of the dye can be recorded continuously with the use of a fluorometer. One disadvantage of the fluorescent-dye method is that a more complex analytical procedure is needed than for the titration method, thus introducing more possible sources for error.

Berl saddles coated with the mixture '99% benzoic acid 1% Rhodamine B' were used in the present experiments to determine the mass transfer characteristics.

DERIVATION OF EQUATION OF $k_S\phi$

To derive the rate equation for mass transfer between the solid particles and the liquid in a three-phase fixed bed, the following assumptions were made:

1. Axial dispersion in the bed is negligible.
2. The surface area of the particles per unit volume in each bed is uniform.
3. The concentration of the liquid in contact with the surface of the solid is the solubility of the solid in the liquid.
4. For any cross section of the bed, the bulk concentration is uniform.
5. k_S is independent of concentration change and is uniform throughout the bed.

Consider the three-phase packed column shown schematically in Figure 1. The tower has a total cross-section area, S, perpendicular to the direction of flow. The total height of the active packed section is Z_B, providing an effective mass-transfer area, a_W, per unit packed volume.

The liquid flow is constant, entering at V_L m/s. While the solid is dissolving, the concentration at the interface is constant at C_S, the inlet bulk concentration of the fluid is C_O, and the outlet concentration is C_1. At pseudo steady-state, over a differential packed height dz a material balance was set up based on a unit area of packing cross-section:

$$N dz = k_S a_W (C_S - C)\, dZ = V_L\, dC \qquad (11)$$

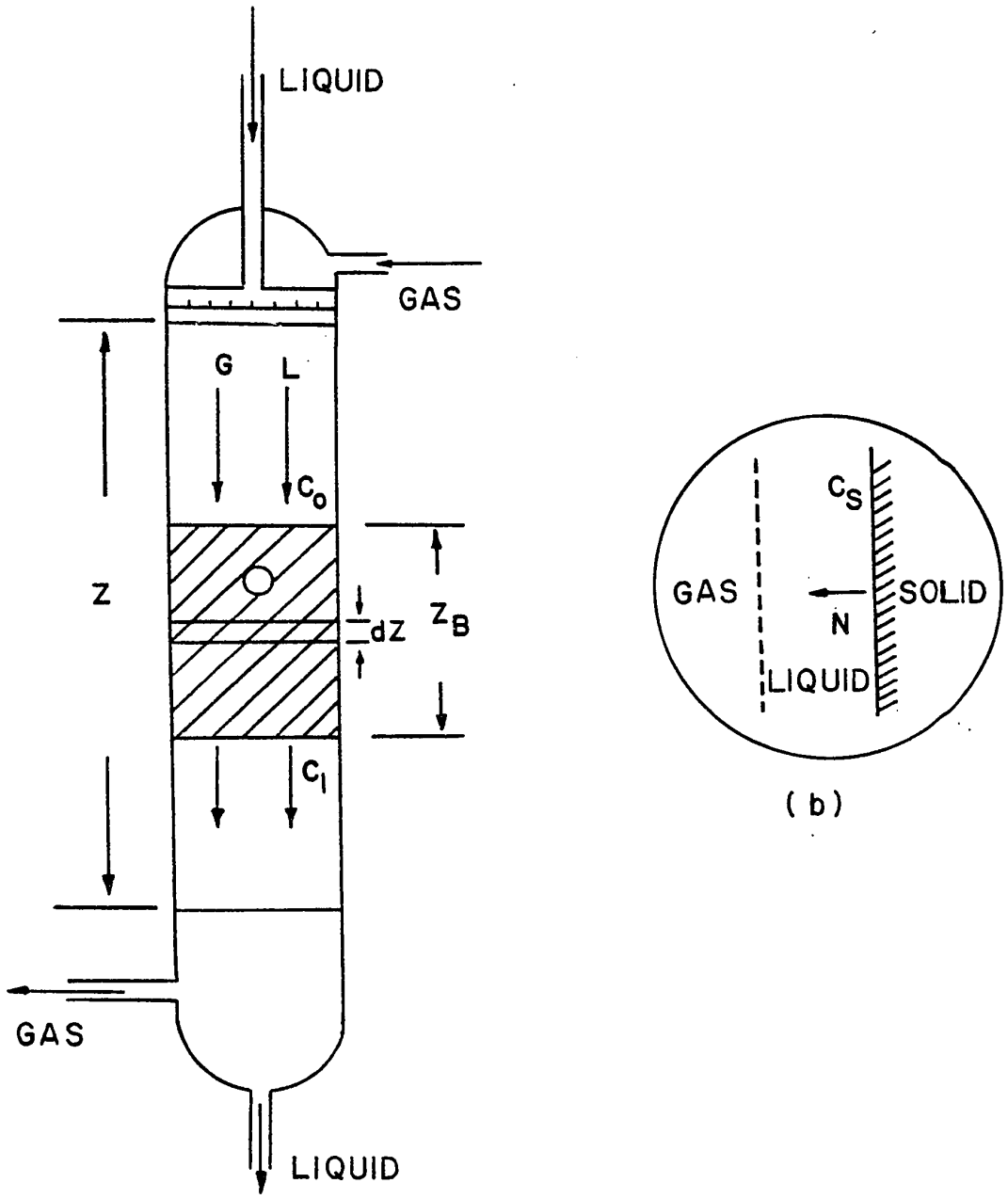

Figure 1. Schematic model of a trickle-bed reactor.

(a) a differential element over which a mass balance is made.

(b) model of mass transfer operation

Integrating this expression between the limits for packing depth of O and Z_B and concentration C_o and C_1 yields:

$$\int_0^{Z_B} k_S a_W dZ = V_L \int_{C_o}^{C_1} \frac{dC}{(C_S - C)}$$

solution for $k_S a_W$ gives:

$$k_S a_W = \frac{V_L}{Z_B} \ln \left(\frac{C_S - C_o}{C_S - C_1} \right)$$

If the inlet bulk concentration C_o is zero, then it follows that:

$$k_S a_W = \frac{V_L}{Z_B} \ln \left(\frac{C_S}{C_S - C_1} \right) \qquad (12)$$

Since a_W is still an obscure value, it is difficult to separate k_S from $k_S a_W$. For this reason the fractional wetted area, a_W/a_S, was used instead of a_W throughout this work (28). Hence, Equation 12 could be modified as:

$$k_S \phi = \frac{V_L}{a_S Z_B} \ln \left(\frac{1}{1 - (C_1/C_S)} \right) \qquad (13)$$

where $\phi = a_W/a_S$.

EXPERIMENTAL SECTION

1. Experimental Apparatus:

The equipment used, shown schematically in Figure 2, was substantially the same as that described in detail by Lemay 1974 (3).

The packed bed consisted of 3 parts having an inside diameter of 0.075 m and a total height of about 0.762 m. The test part was set at about 0.56 m from the top of the packed bed in order to avoid upper end effects. The inert entrance part and the inert exit part were packed with 6.35 mm Berl saddles obtained from the Maurice A. Knight Company, which supplied the specifications shown in Table 1.

The gas and liquid inlet distributor, above the packing, was constructed as follows: 50 stainless steel tubes with an inside diameter of 0.16 cm were arranged in the distributor to introduce the gas flow uniformly over the tower cross section. It also had a total 190 of holes 0.4 mm in diameter on the bottom portion of the distributor designed to give a uniform liquid distribution to the packing. A diagram is given

Table 1. Characteristics of sample packing

Packing	Nominal size (in.)	No. of pieces per ft^3	Porosity (%)	Surface Area a_V ft^2/ft^3
Berl saddle	1/4	113,000	63	274

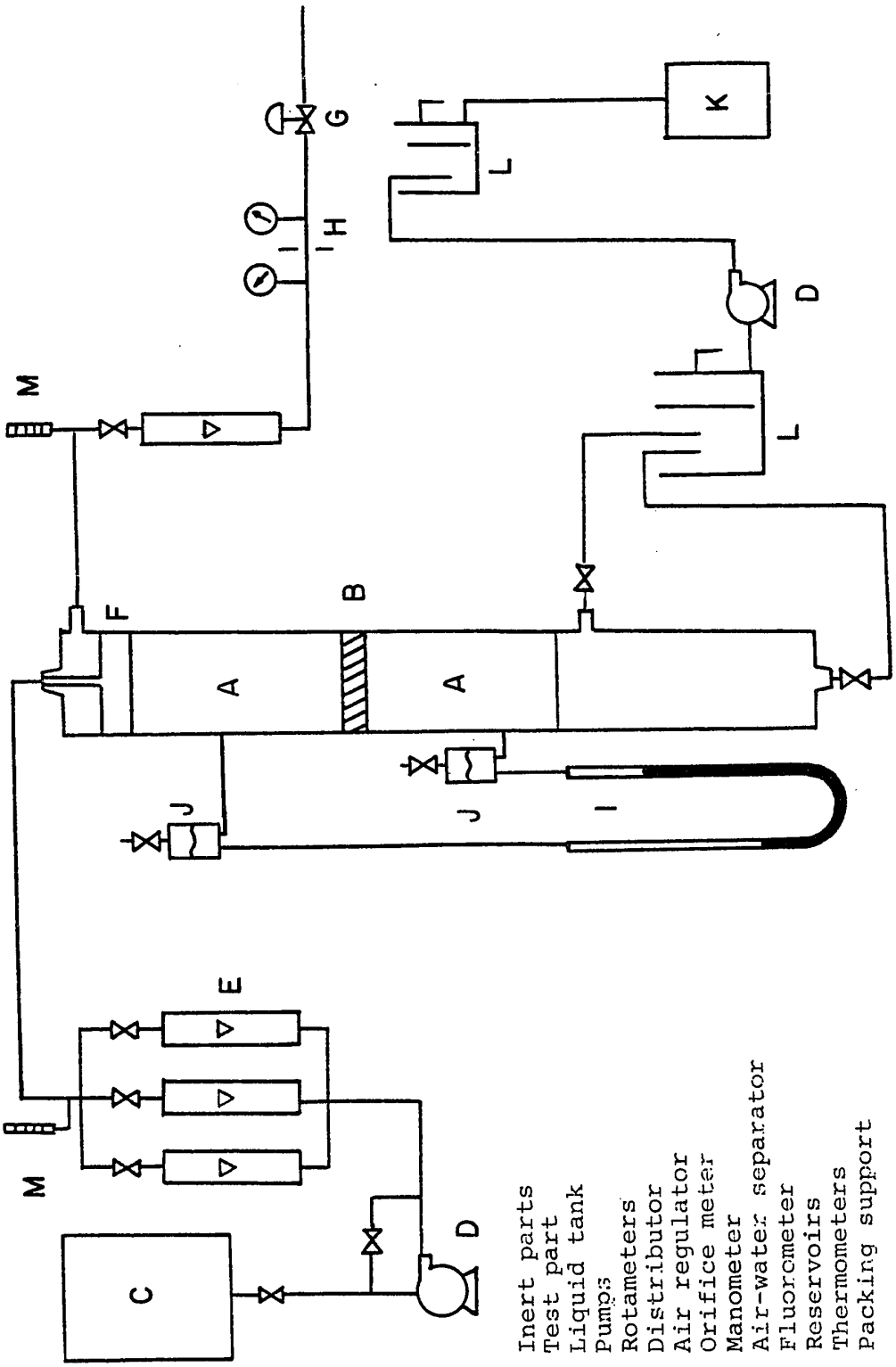

Figure 2. Experimental Apparatus

in Figure 3. Because the nature of the packing support has a definite effect on the flow characteristics in a packed tower, care was taken to design a support which had a greater free area than that of the particles supported. A plastic grid covered with a stainless steel wire screen having 1.5 mm openings was used as a support.

Two pressure taps were located at points 0.20 m and 0.7 m from the top of the packed bed. A manometer was connected to these to measure the pressure drop across the packed bed. In order to keep the manometer from becoming partly filled with liquid and partly with gas, and thereby giving rise to errors in the manometer reading, a gas-liquid separator was connected to the upper pressure point, as shown in Figure 2. Any small air bubble trapped in the manometer line was thus readily separated in the upper part of the separator, and the pressure lines were filled with water.

Air, taken from the laboratory supply line, was reduced in pressure to 24 psig with an air pressure regulator. The air rate was metered by a sharp-edged orifice, mounted in a 1.4 cm diameter pipe. The opening in the orifice plate was 0.65 cm. Equations for calculating the air flow rate were obtained from the fourth edition of the Chemical Engineer's Handbook (12).

Water was supplied from a storage tank and was pumped through the system by means of a gear pump. The water was initially directed through one of three rotameters, which were calibrated by measuring the quantity of water flowing through

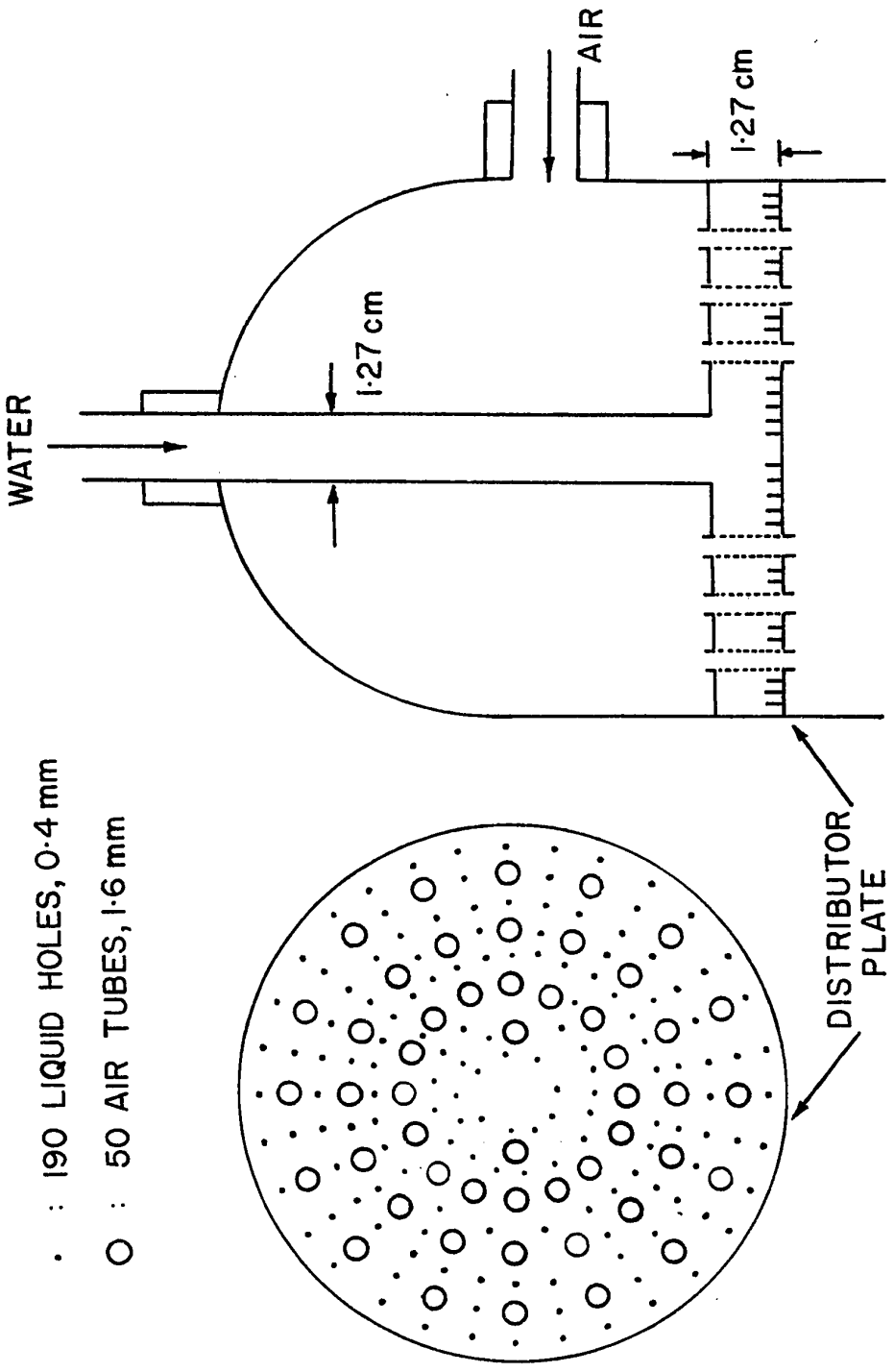

Figure 3. Gas-liquid inlet distributor

them. Three rotameters were used because of the wide range of liquid flow rates utilized in the experiments. The liquid flow rate was controlled by means of a globe valve in the water line.

A plastic reservoir was connected to the liquid exit piping to collect and temporarily store a sample of the effluent solution. The reservoir was partially separated into two parts by a plastic plate, allowing liquid flowing from the bottom to be piped into either part. The solution was then pumped to a smaller reservoir which had the same structure as the first one and which was placed 1 m higher in elevation than the detector of the fluorometer. This latter tank was used to separate air bubbles from the liquid and to maintain a constant flow rate for the liquid entering the detector. The level of the solution was kept constant by means of a hole near the top of the reservoir to drain the excess of solution.

The concentration of dye in the sample was measured continuously by a Turner III fluorometer equipped with filter No. 110-832 and 110-820. Readings were taken by means of a recorder which was connected to the fluorometer.

II. Preparation of Packing Materials:

Benzoic acid was first melted by means of a heating tape and a hot plate as shown in Figure 4. The temperature was controlled at 128°C, a melt temperature which was found to give a uniformly coated film on the Berl saddles of approximately 0.3 mm in thickness. Then the dye (Rhodamine B) was added to the melted benzoic acid to make about 1 wt. % solution. The solution was stirred until uniform, and each of the Berl saddles

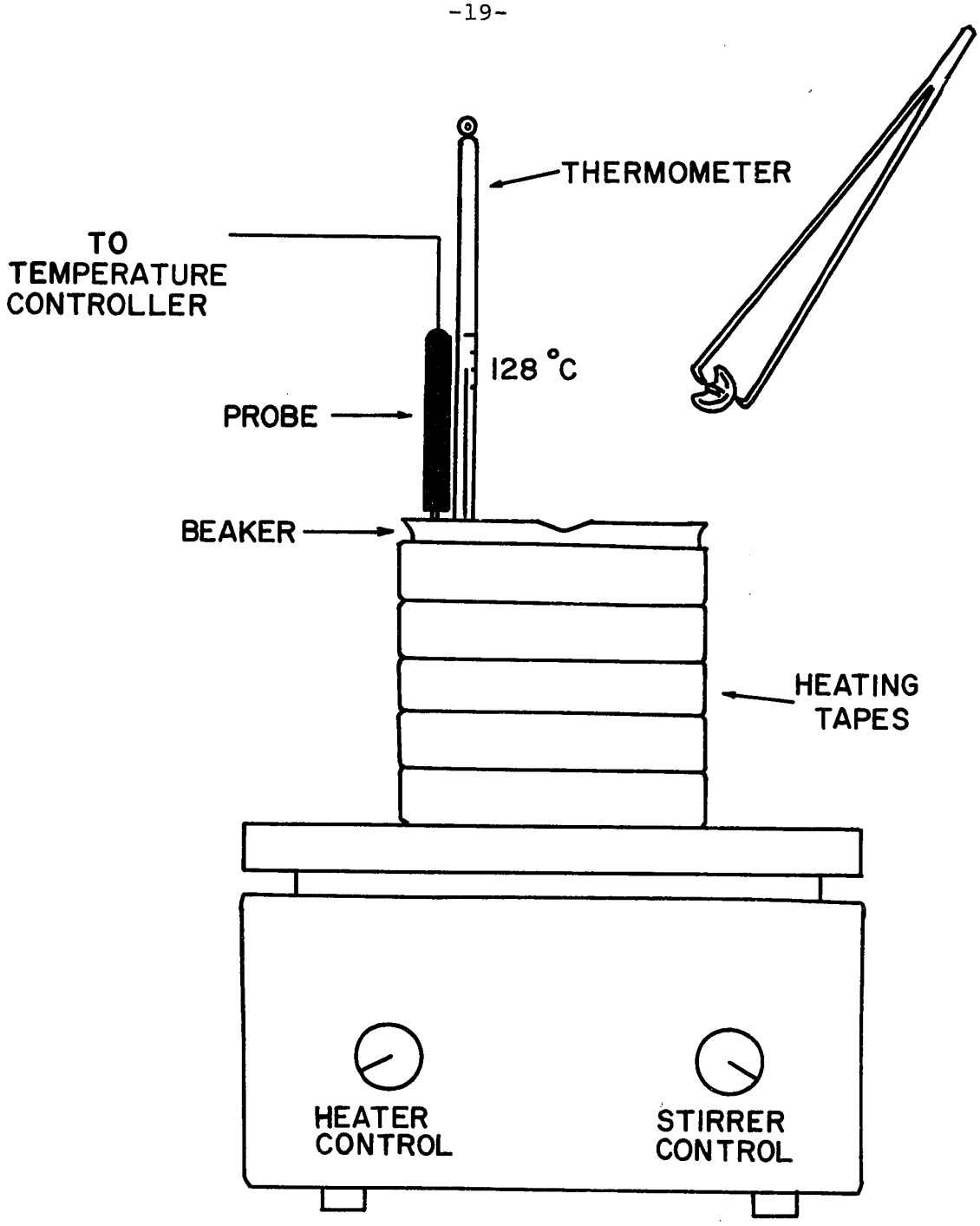

Figure 4. Coating Apparatus

was individually dipped in the solution for a few seconds. Owing to the vaporization of the solution during the coating process, the concentration of the solute was subject to possible change. Some of the melted solution was therefore taken before and after the coating process to measure the ratios of benzoic acid to Rhodamin B. The measurements were averaged, and this average was used for subsequent analysis.

III. Measurement of the Ratio of Benzoic Acid to Fluorescent Dye in Coated Berl Saddles

The sample of solid dye-benzoic acid mixture was first completely dissolved in distilled water and the concentrations of both solutes were separately determined to avoid any possible error resulting from moisture in the sample.

The concentration of dye was measured with the fluorometer which had been calibrated using known concentrations of dye. The concentration of benzoic acid was analyzed by titration with a 0.01 N sodium hydroxide solution which was frequently renewed to prevent a buildup of carbonate because of CO_2 absorption from the air. The 0.01 N sodium hydroxide solution was prepared by diluting a 1 N prepared standard solution which was obtained from the BDH Chemicals.

The sodium hydroxide solution was standardized with a benzoic acid solution, which was prepared as follows: pure benzoic acid was melted by heating the acid to a temperature of 130°C in order to evaporate any water that might have been present because of the hygroscopic nature of the acid. After cooling, some benzoic acid was weighed and then dissolved in

20 ml of ethyl alcohol. This solution was then titrated with the solution to be standardized. A pH meter was used to indicate the end point. The end points were determined by a tabulation method (8) which is based on the fact the first differential quotient at the point of inflexion of a titration curve yields a maximum value and the second differential quotient yields a value of zero at the same point. The method of determining the end-point volume is illustrated by the following example:

Table 2. Data from a titration of 50 ml of benzoic acid solution vs. 0.01 N NaOH

Volume of base ml	pH	Δ^1pH	Δ^2pH
7.80	5.70		
		0.30	
8.00	6.00		0.43
		0.73	
8.20	6.73		1.49
		2.22	
8.40	8.95		-1.67
		0.55	
8.60	9.50		-0.25
		0.30	
8.80	9.80		

The maximum value of Δ^1pH in the above table is 2.22 which appears between the volume values of 8.20 and 8.40, hence the end point falls between these two values. The end-point volume can be determined by using the following calculation where the volume added in each step was 0.2 ml:

$$\text{End-Point-Volume} = 8.20 + (0.2)\left(\frac{1.49}{1.49 + 1.67}\right)$$

$$= 8.29 \text{ ml}$$

After both concentrations had been determined, the ratio of benzoic acid to dye was calculated. Figure 5 shows the titration apparatus.

IV. Preparation of Fluorometer:

The fluorometer was first warmed up for at least 30 minutes in order for it to reach steady-state. Water obtained from the water storage tank was used as the blank solution. The fluorometer was adjusted with the blank knob so that the blank solution gave a zero reading on the recorder. The fluorometer was calibrated with standard solutions prepared with the same water for all runs. This analysis procedure for benzoic acid was quicker and easier to perform than the titration procedure.

V. Measurement of Surface Area:

The surface area of Berl saddles coated with benzoic acid-dye mixture was measured by means of a technique in which glue and metal powder were used. This method has been proven valid in measuring the surface area of spheres within an error of 6% as shown in Table 3.

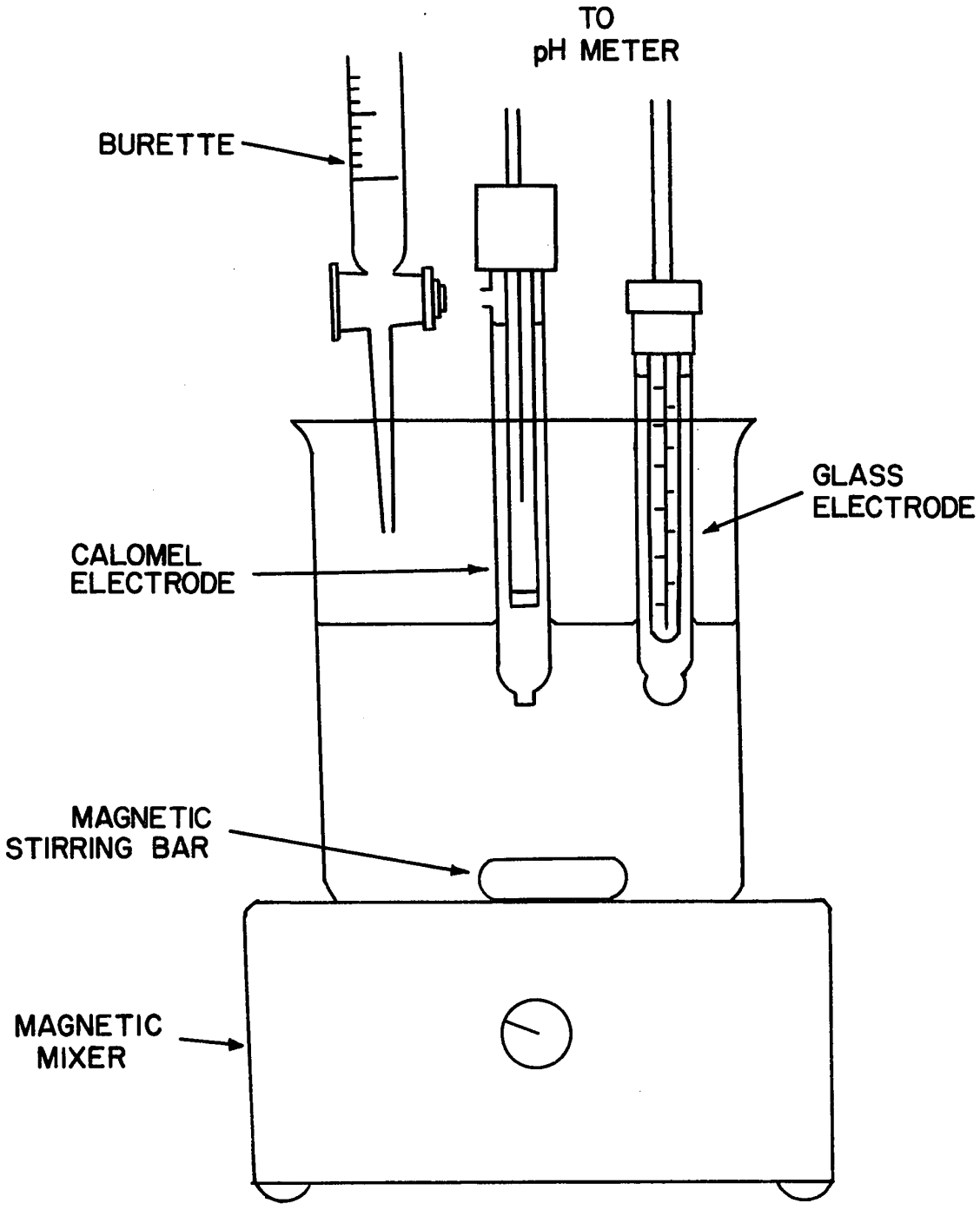

Figure 5. Titration Apparatus

The glue used in this study was obtained from Lepage's Limited and was diluted with an equal volume of butylacetate. Each sample whose area was to be measured was dipped into the glue solution and allowed to drain. Then it was allowed to dry for 125S, when the glue just became tacky, and then it was weighed. Next it was rolled in fine metal powder, so that it picked up a fine even coat, and was weighed again. The difference between the initial and the final weight was the weight of the coat of metal power. If this amount was measured for one particle (sample 1) and then for another particle of the same shape but of a different size (sample 2), the ratio of the weight of the metal power coat on the two particles is equal to the ratio of the two areas. If the surface area of sample 1 is known, that of sample 2 can thus be found.

Table 3. Measurement of surface area of spheres by using glue method

True surface area, cm^2	Weight of coated metal powder, g	Surface area measured, cm^2	Error %
3.37*	0.1172	3.37	0
3.29	0.1084	3.12	5.26
3.45	0.1225	3.52	2.03
6.68	0.2384	6.86	2.62
6.65	0.2218	6.38	5.01

* Reference sample

In this study, sample 1 was taken to be a previously uncoated Berl saddle, having the surface area reported by the production company. Sample 2 was a Berl saddle coated with benzoic acid-dye mixture.

A random sample of 50 was taken to measure the surface area. The average surface area for the coated Berl saddles was found to be 3% higher than that of the bare Berl saddles.

VI. Preparation of Packed Bed:

Water was introduced into the column through the top until approximately 70% of the height of the column was filled. The packing was carefully poured into the column from a container up to a depth of 0.2 m. A layer of coated Berl saddles (150 of them) were then placed on top of the packing, distributed uniformly over the cross section of the columr. This was covered by additional packing, which extended to 1 cm below the distributor. The tower was drained and then closed.

VII. Operating Procedure:

All mass transfer runs were performed at a temperature of 24.5$\pm$ 0.5°C and at normal atmospheric pressure. Air was first fed from the top of the column at the desired flow rate and then water was introduced at the desired flow. The two phases flowed cocurrently downward through the packed bed. The air was exhausted to the atmosphere at the bottom of the column and the liquid directed to the first reservoir. The liquid solution was pumped upward into second reservoir and allowed to flow downward to the fluorometer at a constant rate

due to the constant difference in height.

Once the recorded reading reached a constant value, i.e. the concentration of the solution was constant, readings for orifice pressure drop, column pressure drop, and inlet and outlet liquid temperature were recorded. After the run had been completed, the water flow was stopped and the air flow rate increased to a value of 1.80 kg/m^2s in order to dry the packing for measurement of the bed porosity.

VIII. Porosity Measurement:

After the packing had been air-dried for 5 hours, the top of the column was opened. Water was introduced at the bottom of the column till it just contacted the bottom of the packed bed. Measured amounts of water were then added to fill the column, to the top of the packed bed. The ratio of the measured volume of water to the volume of the packed bed was the porosity of the bed. Since the test section was only a small part of the packed bed, the decrease in volume of the packed bed during a run could be neglected.

EXPERIMENTAL DATA AND CALCULATION

The liquid temperature varied less than 0.6°C through the system during an experimental run. The average temperature was used to calculate the physical properties of the fluids. A decrease of less than 3% of the initial weight of the coated particles for a run was experienced. Since it was difficult to measure a small change in surface area by using the glue method, the surface area as listed in Table 1 was eventually used as representative of the interfacial area in this investigation. The solubility data for benzoic acid in water were those used by Ishine (34) which can be represented by the following equation as a function of temperature:

$$C_S = 1.7 + 0.0197\ t + 0.0020\ t^2 \qquad (14)$$

(t: 0°C to 30°C)

Diffusivity data for benzoic acid in water at 25°C was taken from that quoted by Sherwood et al. (11). Diffusivities at other temperatures were extrapolated by using Hayduk's equation (19). The results of the extrapolation are shown in Table 4. Viscosity and density data for water were taken from Chemical Engineer's Handbook (12).

Table 4. Diffusivity of Benzoic Acid in Water

Temp. °C	23	24	25	26
$D*10^5, cm^2/s$	0.949	0.975	1.000	1.026

The range of the various variables covered in the

present work is given in Table 5.

Equation 15, as derived in Appendix I , was used to calculate the surface area of mass transfer for benzoic acid on a coated Berl saddle:

$$A = A_p \ (r \ / \ r + 1) \tag{15}$$

In the above expression r is the ratio of benzoic acid to dye on the particle. The interfacial area per unit volume of packing is obtained from:

$$nA = a_S Z_B S, \tag{16}$$

In the above expression n is the total number of the coated Berl saddles in the test part and S is the cross-section of the column. Equation 13, can be modified as:

$$k_S \phi = \frac{V_L S}{nA} \ln \left(\frac{1}{1 - (C_1/C_S)} \right) \tag{17}$$

A sample calculation for run 20 is given below:

Table 5. Range of the Parameters Covered

1.	Particle shape: 6.35 mm Berl saddles coated with with benzoic acid mixture.	
2.	Effective particle diameter*, d_p, m,	:0.00847
3.	External area of a single particle, A_p, cm^2,	:2.258
4.	External particle area per unit volume of bed, a_V, m^2/m^3,	:0.0899
5.	Column diameter, m,	:0.0754
6.	Void fraction, ε, %,	:59.3-63.5
7.	Average temperature, °C,	:23.4-25.2
8.	Water flow rate, L, $kg/m^2 sec$,	:2.1 -97
9.	Air flow rate, G, $kg/m^2 sec$,	:0.33-1.77
10.	Modified Reynolds number, Re'_L,	: 16 -460
11.	Schmidt number, Sc,	:887 -931

* The effective particle diameter, d_p, was defined (10) as the diameter of a sphere having the same surface area as the particle; that is, $d_p = \sqrt{A_p/\pi}$. (18)

Average temperature, °C, : 25°C

Water flow rate, m/sec, :0.02125

Solubility of benzoic acid in water, C_S, g/l, :3.443

Ratio of benzoic acid to dye, r, :110

Concentration of dye, $C_D * 10^4$, g/l :8.514

Concentration of benzoic acid, $C_1 = C_D * r$, g/l :0.0911

Surface area of mass transfer for benzoic acid,

$A = A_p (r/r + 1)$, cm^2, :2.237

Number of coated Berl-saddles in the test part, n, :150

$$k_S\phi = \frac{0.02125 * 44.696 * 10^{-4}}{2.237 * 10^{-4} * 150} \ln \left(\frac{1}{1 - (0.0911/3.443)} \right)$$

$$= 7.59 * 10^{-5} \text{ m/sec.}$$

The computed variables derived from the experimental measurements including $k_S\phi$, Re_L, $Sh\phi$, Sc, Re_L', $Sh'\phi$, J_D for all runs are presented in Appendix III(Table 6,7,8,9,10,11).

RESULTS AND DISCUSSIONS

Figure 6 shows the boundaries of the hydrodynamic flow regimes as obtained in this work and the flow rates chosen for the measurement of k_s in the experiments.

The pressure gradient, $(-\Delta P/Z)_{LG}$, was calculated by means of Equation 19 which did not require a knowledge of the vertical distance (Z) between the taps nor the density of the fluid used in the lower part of the manometer (7):

$$(-\Delta P/Z)_{LG} = g\rho_L \left(\frac{R-R_O}{R_O}\right) \qquad (19)$$

In the above expression R and R_O were the readings of the manometer with and without flow in the column and ρ_L was the density of the liquid in the pressure line and the arms of the U tube as shown in Figure 7.

It should be noted that during the pulsing flow regime the pulses passing through the column caused pressure pulsation (4,5). An arithmetical average of the readings was used in this work.

The experimental results of the pressure gradient $(-\Delta P/Z)_{LG}$ versus G, with liquid flow rate as a parameter is plotted in Figure 8. The result clearly shows that the slopes of the solid line decrease with increasing liquid flow rate and tend to approach the extended line of zero liquid flow rate with increasing gas flow rate. This pattern is in general agreement with the pressure gradient reported by Dodds et al. (9) with 1 in Berl saddles. This appears reasonable, because with a high gas flow rate the liquid film becomes thin

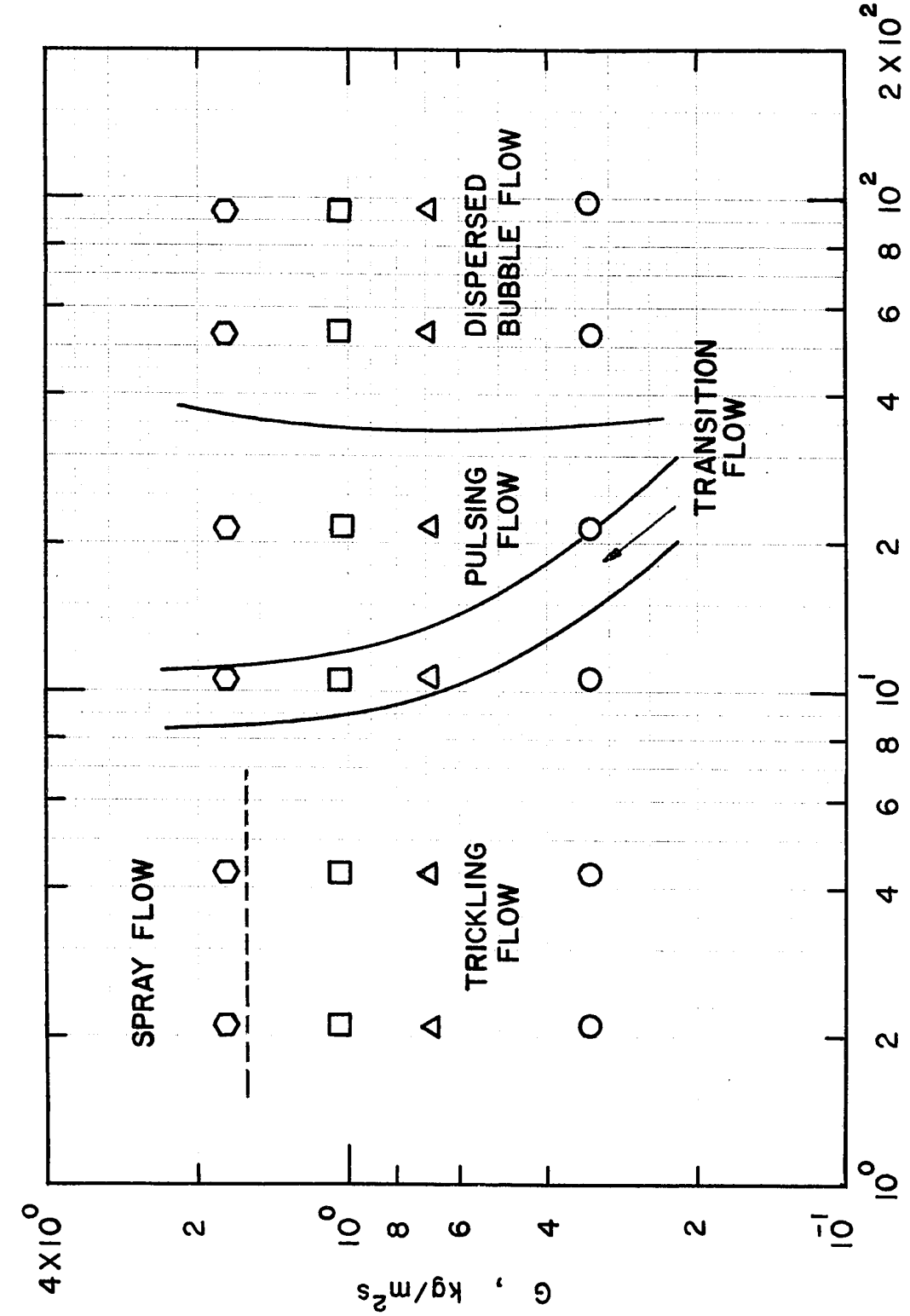

Figure 6. Experimental data points and boundaries of flow patterns

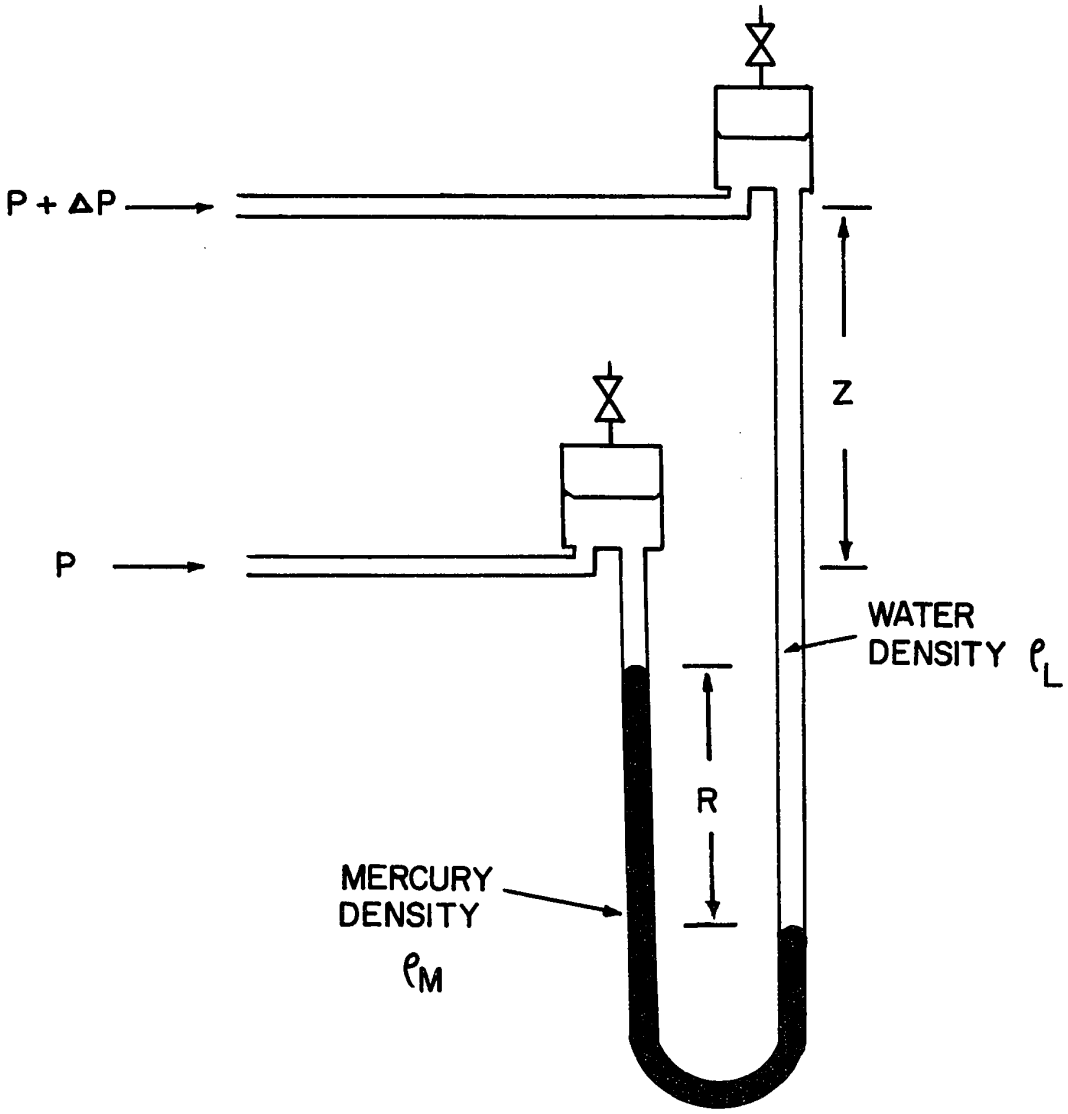

Figure 7. Schematic Diagram of Manometer

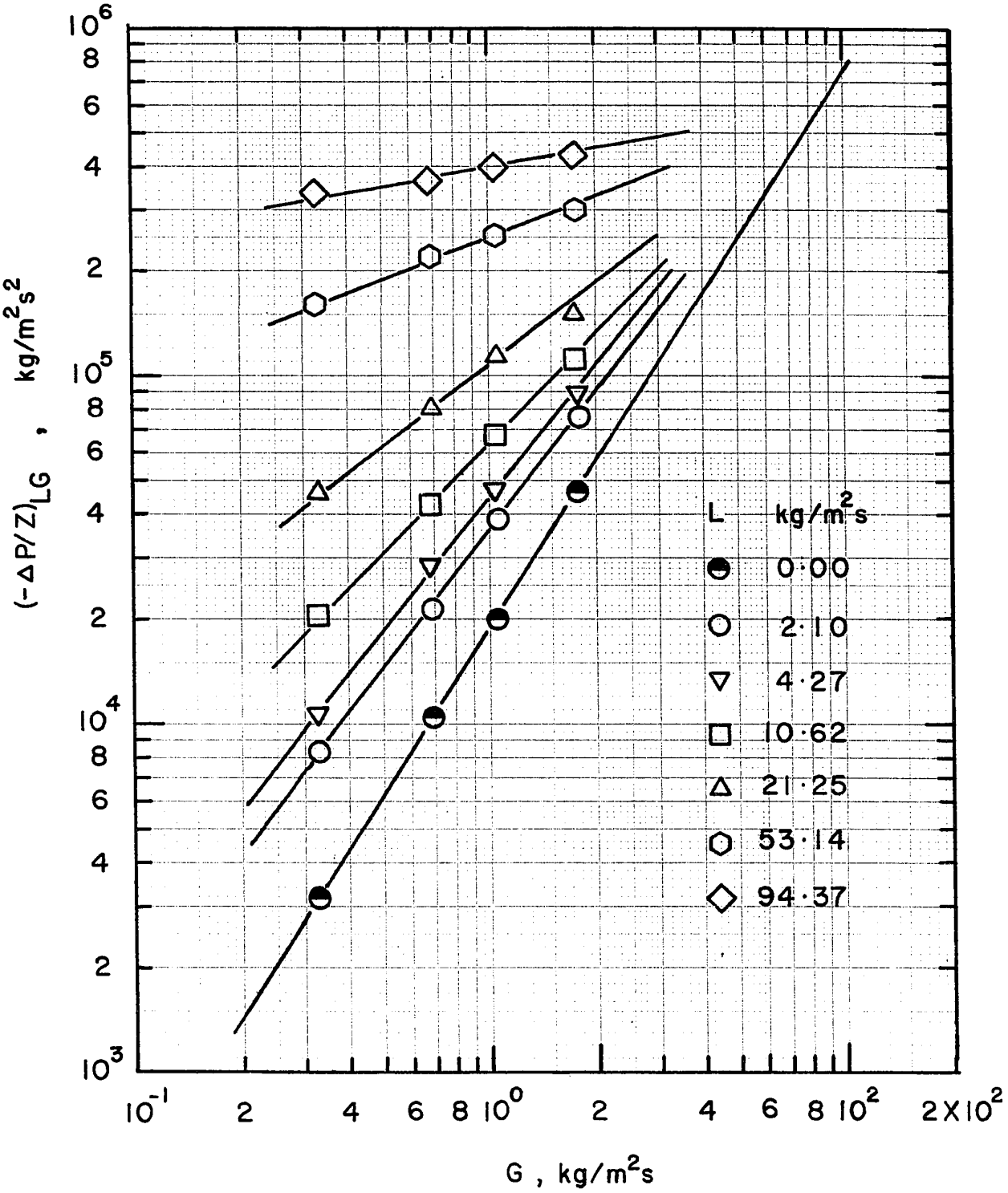

Figure 8. Two-phase pressure drop in packed bed

and its influence on the gas flow rate tends to disappear.

Values of $k_S\phi$ as influenced by the gas and liquid flows are presented in Figure 9 and 10. The general shape of the curves is similar to that reported by Hirose et al. (13). It is clearly shown that the lines connecting the values in Figure 9 lie above the correlation curve for a liquid phase flowing through a packed bed in the absence of a gas flow (13). This enhancement becomes more significant in the pulsing flow regime.

At a low Re_L and low gas flow rate, resulting in a trickling flow, the $sh\phi$ is slightly influenced by the gas flow rate but increases with Re_L to about the 0.58 power. This is also the conclusion of previous investigators (13,14, 28) and can be reasoned by reference to the fact that in the trickling flow the gas flow is too low to spread the liquid sufficiently over the packing and hence part of surface remains unwetted. Liquid phase flows down as a laminar film. Hirose et al. (13) reported that in spray flow, the effect of gas flow on mass transfer rate became more significant. This can be explained that at high gas flow rate , part of the liquid is suspended as a mist in the gas stream and the extent of wetting of the packing surfaces increases and the packing is coverd with a turbulent layer of liquid. The turbulent film and larger wetted surface may be responsible for an increase in the mass transfer rate.

Specchia et al. (14) found that for a given liquid flow rate, an asymptotic value of k_S would be obtained as the

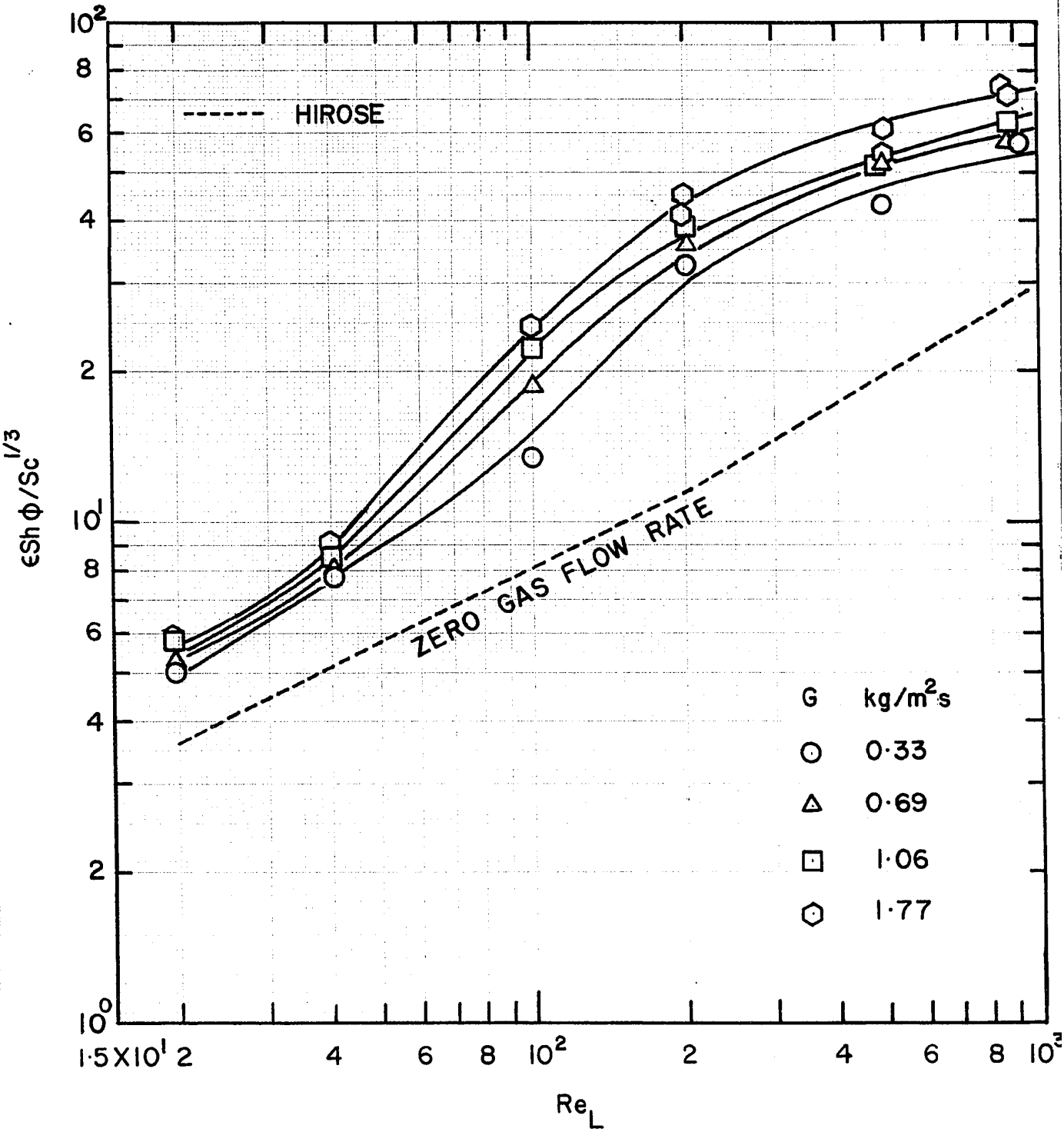

Figure 9. Effect of Re_L on $\varepsilon Sh\phi/Sc^{1/3}$

gas flow rate was increased.

For the transition and pulsing flow regimes Figure 9 suggests that the relation between the variables can be expressed by a convex curve rather than a straight line. The mass transfer rate increases rapidly with an increase in either the gas flow rate or the liquid flow rate. It can also be seen in Figure 10, that the slopes of the correlating lines, essentially relating the mass transfer coefficient and gas flow rate, hence the exponents to be attached to gas flow rate, are greater for the transition and pulsing flow regimes than for the other regimes. This trend may be brought about not only by greatest utilization of the particle surface area but also by the much higher speed of the pulses with respect to the actual velocity of the liquid phase (15), producing a higher stress on the solid surfaces.

With a further increase in the liquid flow rate resulting in dispersed bubble flow regime, the gas rate became a less important factor in determining the mass transfer rate. Sylvester et al.(16) found that $k_S\phi$ became independent of the liquid rate at liquid fluxes greater than 8.6 kg/m^{2}s, corresponding to the transition flow regime. Because of the limitations of the gear pump used in the present experiments, liquid flows could not be generated at a rate high enough to reach this point. However, this value was not found by Sato et al. (30), Lemay et al. (3) nor by Hirose et al. (13) either. Finally, Figure 10 shows that the influence of the gas flow rate on the mass transfer rate becomes least important in the dispersed-bubble flow regime.

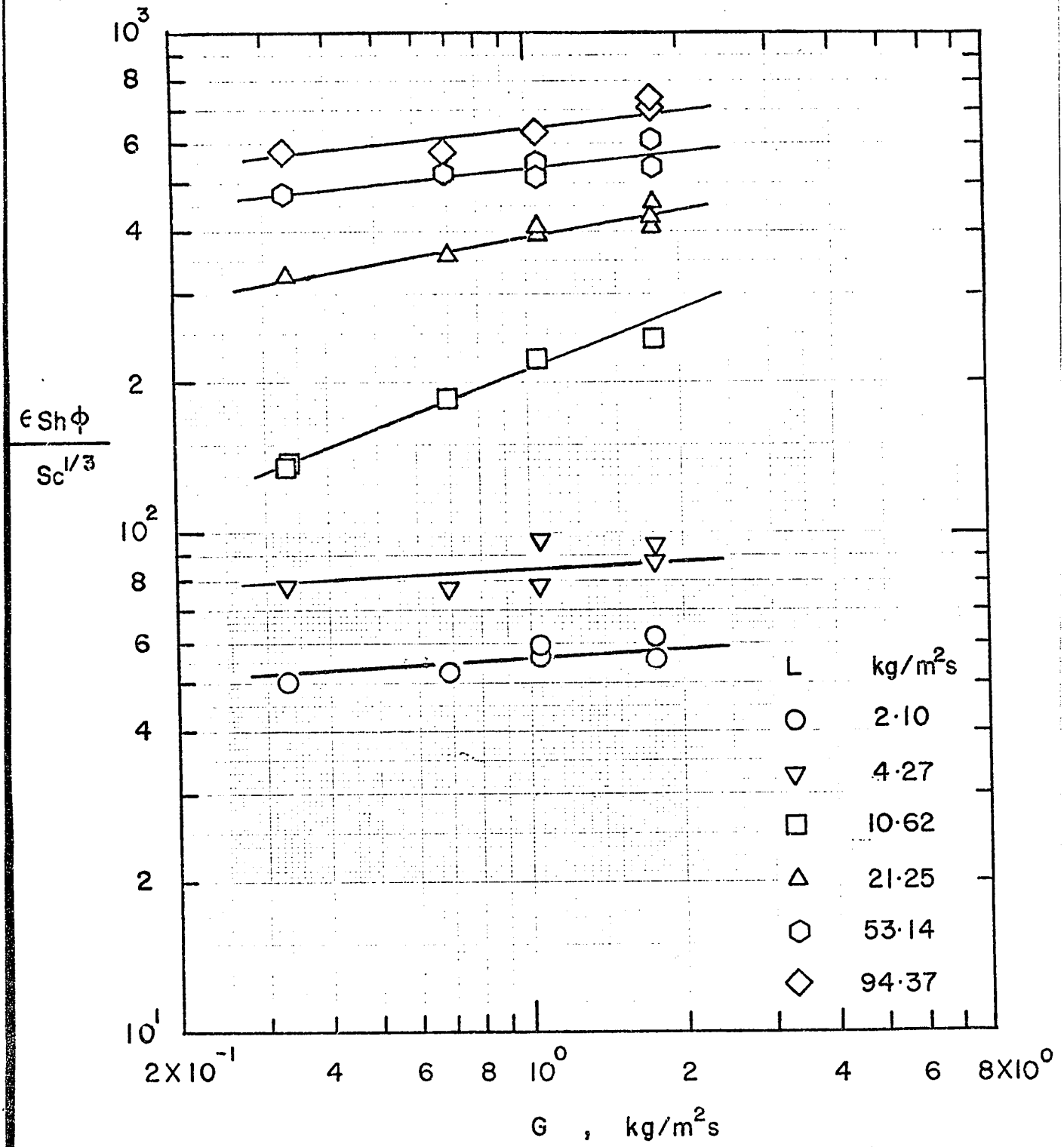

Figure 10. Effect of gas flow rate on $\varepsilon Sh\phi/Sc^{1/3}$

CORRELATION OF RESULTS

In correlating their results, previous investigators have taken several approaches.

Dharwadkar et al. (17) correlated their data and those of others (13,16,2,30,31,32) in terms of the mass transfer factor, J_D, and the particle Reynolds number defined previously. Their resulting equation is:

$$J_D = 1.637\ (Re_L)^{-0.331} \qquad (0.2 < Re_L < 2400) \qquad (20)$$

The mean, and standard deviation were 7.14 and 0.28% respectively. The J_D factor versus Re_L plot for the data produced in this research is shown in Figure 11, along with the dotted line representing Equation 20. This plot clearly indicates that the data for the pulsing flow regime is best represented by a convex rather than a straight line. The best simple exponential equation to be applied to the data is given by:

$$J_D = 1.254\ Re_L^{-0.315} \qquad (21)$$

It can be seen from Figure 11 that there is a considerable scatter in the data when represented by a J_D-Re_L plot. Therefore it appeared useful to consider the influence of gas flow on the mass transfer rate.

Lemay et al. (31) correlated their data in the pulsing flow regime by an equation of the Calderbank and Moo-Young form (29), which assumed that $k_S\phi$ was proportional to $D^{2/3}$ and independent of d_p:

$$k_S\phi Sc^{2/3} = 0.20\ (E_L'\mu_L/\rho_L)^{1/4} \qquad (22)$$

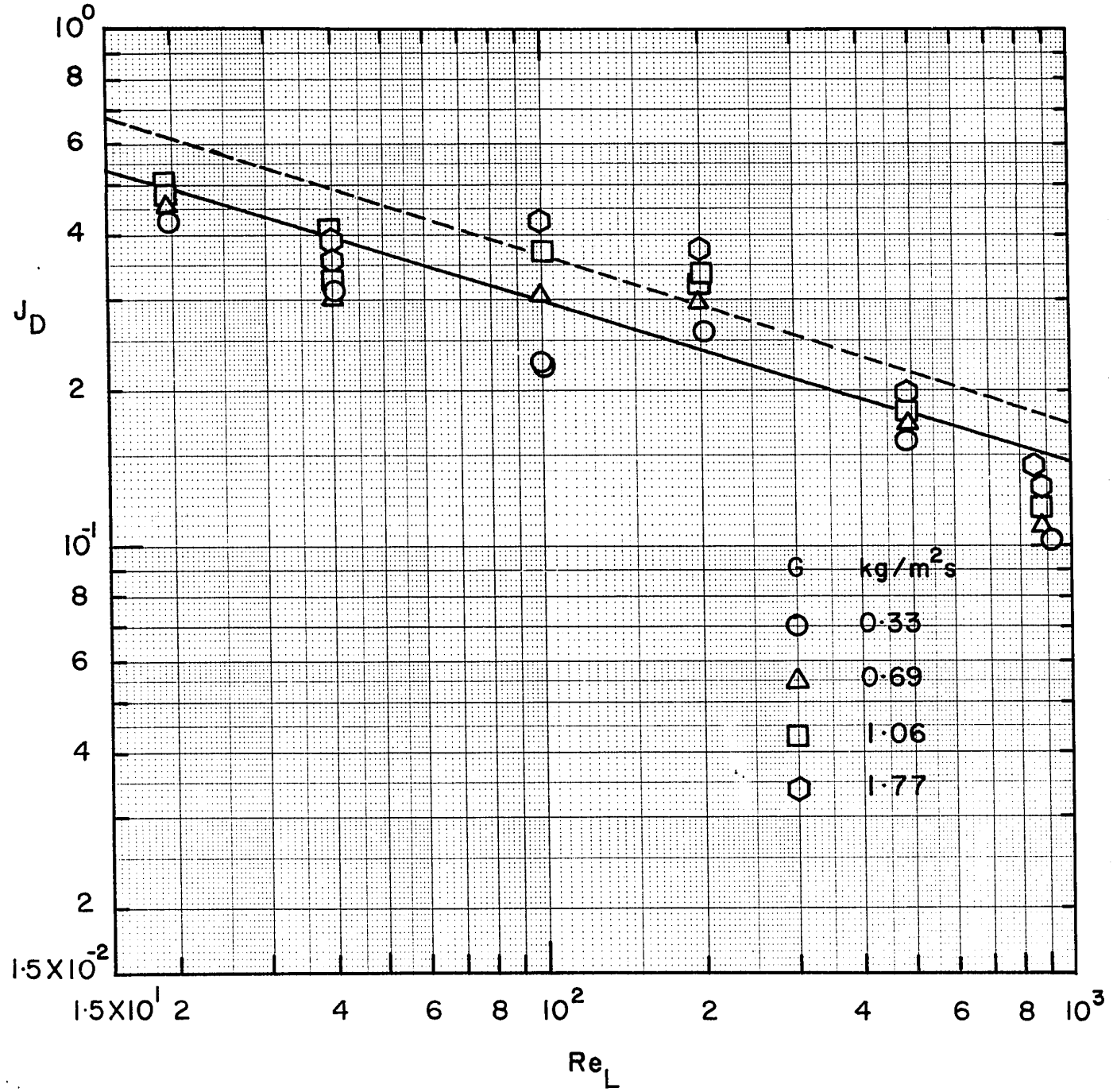

Figure 11. J_D factor vs. Re_L correlation of the experimental data.

where

$$E_L' = E_L / h_L\rho_L = \frac{(-\Delta P/Z)_{LG}\, V_L}{h_L\rho_L}$$

The liquid power dissipation, E_L, was first defined by Reiss (33) and had previously been used to correlate $k_L.a$ in the pulsing and spray flow regimes. It was of interest to see how Lemay's correlation (31) could be applied to the wide range of liquid flow rate covering the four flow patterns. The results are illustrated in Figure 12. It is evident that Lemay's correlation fits the data well in the pulsing and dispersed bubble flow regimes. However, it does not yield a single line for the gas continuous flow regime, but instead a series of lines with the liquid flow rate as a parameter. It would appear, therefore, that Equation 22 obtains good correlation in only the pulsing and dispersed bubble flow regimes. The solid straight line in Figure 12 corresponds to the following equation, obtained by a least-squares regression analysis:

$$k_S\phi Sc^{2/3} = 0.135 \left(\frac{E_L'\mu_L}{\rho_L}\right)^{0.219} \qquad (23)$$

Recently, van Eek et al. (28) reported findings which involved the use of 3 and 6 mm benzoic acid cylinders in the pulsing flow regime and correlated their data in the Calderbank, Moo-Young form. However, their results did not agree well with Lemay's equation. They then assumed that k_S was dependent on d_p and modified Calderbank, Moo-Young's equation into the following form:

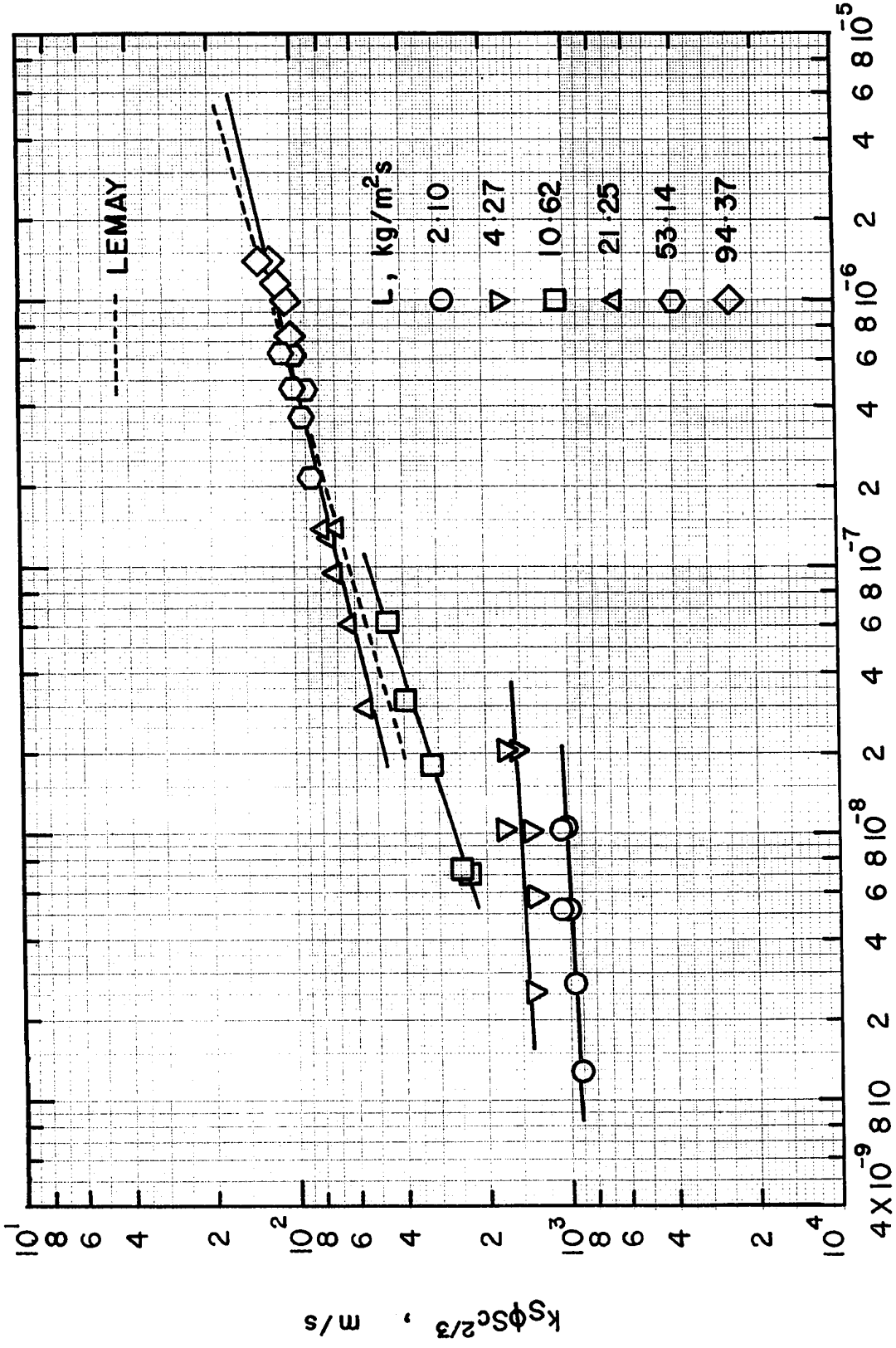

Figure 12. Effect of $E'_L\mu_L/\rho_L$ on $K_S\phi Sc^{2/3}$

$$\frac{k_S \phi d_p}{D} = m \left(\frac{E_L' (d_p)^4 \rho_L^3}{L^3} \right) \left(\frac{\mu_L}{\rho_L D} \right)^{1/3} \quad (24a)$$

or $Sh\phi = m\, Ko^n Sc^{1/3}$ (24b)

In the above expression m and n are constants and Ko is the Kolmogoroff number. Their data were best expressed as:

$$Sh\phi = 0.334\ Ko^{0.202}\ Sc^{1/3} \quad (25)$$

If the Calderbank, Moo-Young assumption that k_S is explicity independent of d_p was true, then n should have been equal to 0.25. However, they found that n was 0.202. It would appear that k_S is slightly dependent on d_p. Figure 13 shows the similar correlation for the data obtained in this work and a comparison with Equation 25 and Lemay's data. A least-squares fit of the data in pulsing and dispersed bubble regimes is given by:

$$\frac{Sh\phi}{Sc^{1/3}} = 0.413\ Ko^{0.220} \quad (26)$$

It is also noted that Equation 25 falls below the Lemay et al. correlation and Equation 26. On the other hand, Equation 26 agrees well with Lemay's equation.

Most of the reported liquid-solid mass transfer data in various types of one-phase-flow packed beds have been successfully correlated in terms of $Sh\phi Sc^{-1/3}$ and Re_L. However, it can be seen from Figure 9 and the data reported by Sato (24) that this kind of approach cannot be used to correlate mass transfer data in a trickle bed reactor into a single band, since the gas

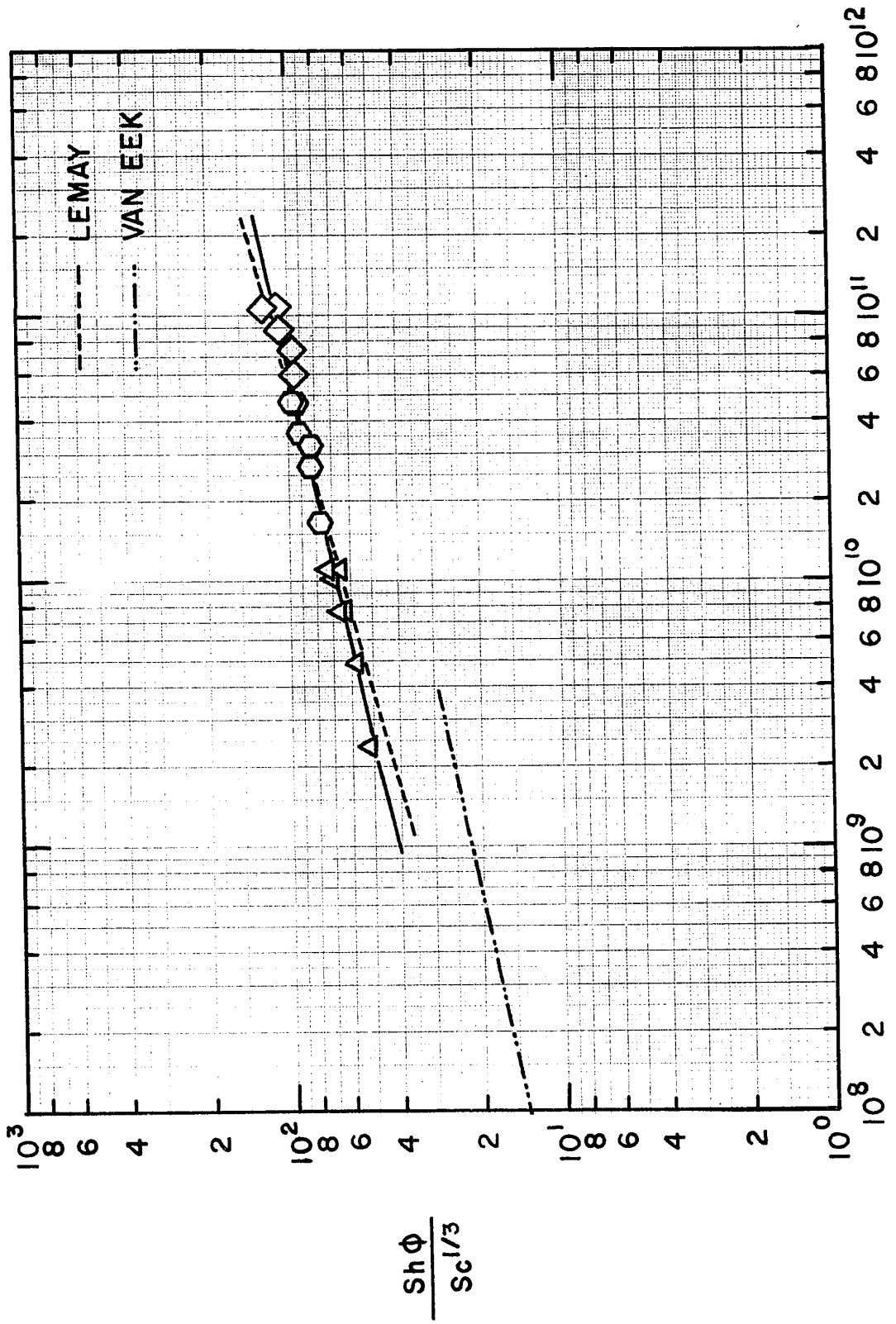

Figure 13. Effect of Ko on $Sh\phi/Sc^{1/3}$

flow rate appears as a parameter.

An attempt was made to correlate the data by taking into consideration the effect of the average actual velocity of the liquid phase in the column represented by:

$$U_L = \frac{V_L}{h_L} \tag{27}$$

The data were converted to the dimensionless group as follows:

$$Re_L' = \frac{V_L \rho_L}{h_L a_S \mu_L} \tag{28}$$

$$Sh'\phi = \frac{k_S \phi}{Da_S} \tag{29}$$

In the above expression the definition of Sh' was the same as that used by Van Krevelen et al. (32) to correlate their data in trickle flow at zero gas flow rate.

When the experimental data is presented by means of the derived dimensionless group $\varepsilon Sh'\phi Sc^{-1/3}$ vs. Re_L', a single band is obtained as shown in Figure 14. The solid lines represent the least-squares fit of these data, given as follows:

$$\varepsilon Sh'\phi = 0.0819\ Re_L'^{\,0.777}\ Sc^{1/3} \quad (Re_L' < 55) \tag{30a}$$

for gas continuous flow;

$$\varepsilon Sh'\phi = 0.00437\ Re_L'^{\,1.517} Sc^{1/3} \quad (55 < Re_L' < 100) \tag{30b}$$

for transition flow;

$$\varepsilon Sh'\phi = 0.680\ Re_L'^{\,0.416} Sc^{1/3} \quad (Re_L' > 100) \tag{30c}$$

for pulsing and dispersed bubble flow.

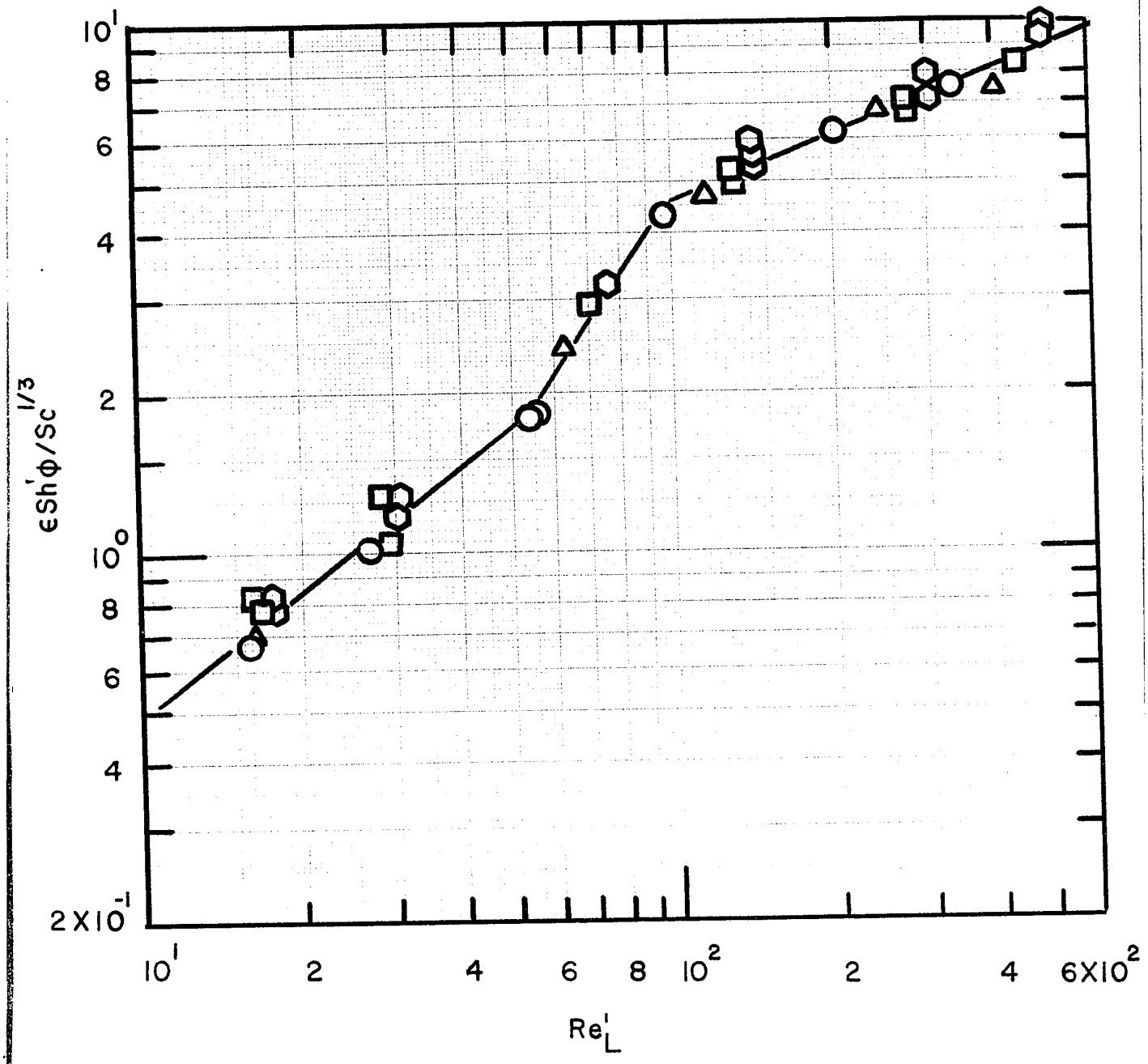

Figure 14. $\epsilon Sh'_\phi/Sc^{1/3}$ vs. Re'_L correlation of the experimental data.

It is apparent that $Sh'\phi$ depends highly on Re_L' in the gas continuous and transition flow regimes. However, there is lesser dependence on Re_L' in the pulsing and dispersed-bubble flow regimes.

It is probable that in the continuous flow regime, both Sh' and ϕ increase as Re_L' increases, and this increase becomes substantial in the transition regime owing to the high degree of turbulence.

It is considered that after the packing becomes completely wetted, a situation which occurs when $\phi = 1$, only Sh' increases with Re_L'. Therefore, the slope of the correlation line changes, corresponding to a change in flow regime.

Lemay's experimental data were also converted to the dimensionless group form as used in Equation 30. Dynamic and static holdup were taken from Specchia et al. (6). Geometric surface areas were calculated by Equation 31:

$$a_S = \frac{6(1-\varepsilon)}{d_p} \tag{31}$$

Figure 15 shows the correlation for Lemay's data and a comparison with Equation 30. The regression line through their data is expressed as:

$$\frac{\varepsilon Sh'\phi}{Sc^{1/3}} = 0.66\ Re_L'^{\,0.41} \tag{32}$$

Goto et al. (2) determined k_S with small β-napthol particles, at low gas and liquid flow rates. Their mass transfer rates were higher in the region of the same Reynolds number than were those found in other reports. Their data for 0.0541 cm

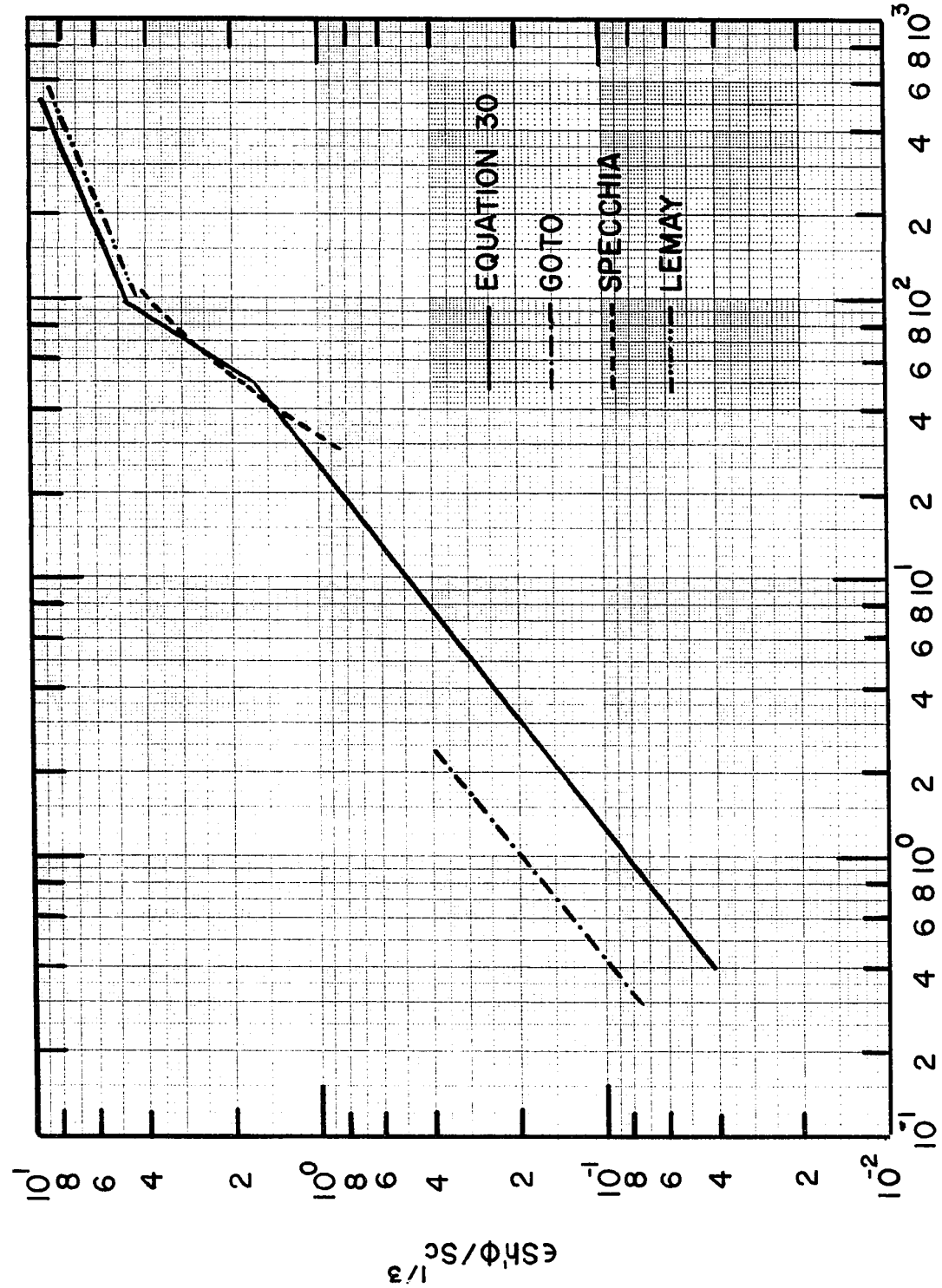

Figure 15. Comparison of correlations

β-naphthol particles were converted into the comparable factors, $\varepsilon Sh' \phi Sc^{-1/3}$ and Re_L', and plotted in Figure 15. The resulting equation can be expressed as:

$$\frac{\varepsilon Sh' \phi}{Sc^{1/3}} = 0.195\ Re_L'^{\,0.790} \qquad (0.3<Re_L'<3) \qquad (33)$$

The mass transfer rates were higher than those obtained by extrapolation of Equation 30. Because of the lack of detail in Specchia's other data (14), only the data obtained with 6 mm benzoic acid cylinders utilized with the air-water system were considered in calculating the corresponding curve in Figure 15 using their equation.

The agreement of the data obtained in this work with the other findings mentioned above seems highly satisfactory, especially when consideration is given to the fact that data were obtained with a number of the different geometries and sizes of the packings. Finally, it is emphasized that if Sh' tended to be independent of Re_L' at a high liquid flow rate as suggested by Sylvester et al. (16), the correlation would be expected to go asymptotically approach a constant value at high Re_L'. However, such a constant asymptotic value was not found in the present study, although the liquid flow rates used were much higher than those of Sylvester. Therefore, more data are needed to establish definitely the shape of the curve at high liquid flow rates.

CONCLUSIONS

1. Mass transfer coefficients are larger for this system than for liquid flowing at a zero gas flow rate. Presumably, gas flow increases the wetting factor, thins the liquid film, and increases the liquid actual velocity and turbulence.
2. For a given liquid flow rate, the effect of the gas flow rate on the mass transfer coefficient is less important in the trickling and dispersed-bubble flow regimes and becomes significant in the transition and pulsing flow regimes. The results are in agreement with those proposed by the previous investigators.
3. The mass transfer data for a moderate range of liquid flow rates has been correlated on a plot of $\frac{\varepsilon Sh'\phi}{Sc^{1/3}}$ vs. a modified Reynolds number $\frac{V_L \rho_L}{h_L \mu_L a_S}$ to yield three lines corresponding to the different flow regimes.

BIBLIOGRAPHY

(1) Østergaard, K., "Gas-liquid-particle operations in chemical reaction engineering", Adv. Chem. Eng. 7, 71 (1968).

(2) Goto, S., J. Levec, and J.M. Smith, "Mass transfer in packed beds with two-phase flow", Ind. Eng. Chem., Process Des. Dev. 14, 473 (1975).

(3) Lemay, Y., "Transfert de matieres liquide-particule dans une colonne garnie" M.A.Sc. thesis, University of Ottawa, Ottawa, Canada (1974).

(4) Weekman V.W., Jr. and J.E. Myers, "Fluid-flow characteristics of concurrent gas-liquid flow in packed beds", A.I.Ch.E. J. 10, 951 (1964).

(5) Sato Y., T. Hirose, F. Takahashi, M. Toda, and Y. Hashiguchi, "Flow pattern and pulsation properties of cocurrent gas-liquid downflow in packed beds", J. of Chem. Eng. of Japan 6, 315 (1973).

(6) Specchia V. and G. Baldi, "Pressure drop and liquid holdup for two phase concurrent flow in packed beds", Chem. Eng. Sci. 32, 515 (1977).

(7) Shearer C.J. and R.M. Nedderman, "Pressure gradient and liquid film thickness in cocurrent upwards flow of gas/liquid mixtures: Application to film-cooler design", Chem. Eng. Sci. 20, 671 (1965).

(8) Dick J.G., "Analytical Chemistry", McGraw-Hill, N.Y. 1973.

(9) Dodds W.S., L.F. Stutzman, B.J. Sollami, and R.J. McCater, "Pressure drop and liquid holdup in concurrent gas absorption", A.I.Ch.E. J. 6, 390 (1960).

(10) Taecker R.G. and O.A. Hougen, "Heat, mass transfer of gas film in flow of gases through commercial tower packings", Chem. Eng. Prog. 45, 188 (1949).

(11) Sherwood T.K., R.L. Pigford and C.R. Wilke, "Mass transfer", McGraw-Hill, N.Y., 1975.

(12) Perry J.H., "Chemical Engineer's Handbook", 4th ed., McGraw-Hill, N.Y., 1963.

(13) Hirose T., Y. Mori and Y. Sato, "Liquid-to-particle mass transfer in fixed bed reactor with cocurrent gas-liquid downflow", J. of Chem. Eng. of Japan 9. 220 (1976).

(14) Specchia V., G. Baldi, and A. Gianetto, "Solid-mass transfer in trickle bed reactors", Paper presented at the 4th International Symposium on Chemical Reaction Engineering, Heidelberg, West Germany, April 1976.

(15) Sato Y., Hirose, F. Takahashi, M. Toda, "Pressure loss and liquid holdup in packed bed reactor with cocurrent gas-liquid down flow", J. of Chem. Eng. of Japan 6, 147 (1973a).

(16) Sylvester N.D. and P. Pitayagulsarn, "Mass transfer for two-phase cocurrent downflow in packed bed", Ind. Eng. Chem., Process Design Dev. 14, 421 (1975).

(17) Dharwadkar A. and N.D. Sylvester, "Liquid-solid mass transfer in Trickle Beds", A.I.Ch.E. J. 23 376 (1977).

(18) Talmor E., "Two-phase downflow through catalyst beds: Part I. Flow map, Part II. Pulsing regime pressure drop", A.I.Ch.E. J. 23, 874 (1977).

(19) Hayduk W. and H. Laudie, "Prediction of diffusion coefficients for nonelectrolytes in dilute aqueous solutions", A.I.Ch.E. J. 20, 611 (1974).

(20) Larkins R.P., R.R. White and D.W. Jeffrey, "Two phase concurrent flow in packed bed", A.I.Ch.E. J. 7, 231 (1961).

(21) Fukushima S. and K. Kusaka, "Interfacial area and boundary of hydronamic flow region in packed column with cocurrent downward flow", J. of Chem. Eng. of Japan 10, 461 (1977).

(22) Turbin J.L. and R.E. Huntington, "Prediction of pressure drop for two-phase, two-component concurrent flow in packed beds", A.I.Ch.E. J. 13, 1197 (1967).

(23) Lockhart R.W., and Martinelli R.C., "Proposed correlation of data for isothermal two-phase, two-component flow in pipes", Chem. Eng. Prog. 45, 39 (1949).

(24) Ergun S., "Fluid flow through packed columns", Chem. Eng. Prog. 48, 89 (1952).

(25) Charpentier J.C. and M. Favier, "Some liquid holdup experimental data in trickle-bed reactors for foaming and non-foaming hydrocarbons", A.I.Ch.E. J. 21, 1213 (1975).

(26) Charpentier J.C.,Thesis, University of Nancy (1968)

(27) Satterfield C.N., "Trickle-bed reactors", A.I.Ch.E. J. 21, 209 (1975).

(28) Satterfield C.N., M.W. van Eek, and G.S. Bliss, "Liquid-solid mass transfer in packed beds with downward cocurrent gas-liquid flow", A.I.Ch.E. 70th meeting, N.Y. (Nov. 1977).

(29) Calderbank P.H. and M.B. Moo-Young, "The continuous phase heat and mass-transfer properties of dispersions", Chem. Eng. Sci. 16, 39 (1961).

(30) Sato Y., T. Hirose, F. Takahashi and M. Toda, "Performance of fixed bed catalytic reactor with co-current gas-liquid flow". First Pacific Chem. Eng. Congress (1972).

(31) Lemay Y., G. Pineault, and J.A. Ruether, "Particle-liquid mass transfer in a three-phase fixed bed reactor with cocurrent flow in the pulsing regimes", Ind. Eng. Chem., Process Des. Dev. 14, 280 (1975).

(32) van Krevelen D.W. and J.T.C. Krekels, "Rate of dissolution of solid substances Part I. Rate of mass transfer in granular beds", Rec. Trav. Chim., 67, 512 (1948).

(33) Reiss L.P., "Cocurrent gas-liquid contacting in packed columns", Ind. Eng. Chem., Process Des. Dev. 6, 486 (1967).

(34) Ishine T., T. Otake, and T. Okaka, Chem. Eng. (Japan) 15, 255 (1951).

(35) Shulman H.L., C.F. Ullrich, and N. Wells, "Performance of packed columns", A.I.Ch.E. J., 1, 274 (1955).

(36) Standish N., "Some observations on the static hold-up of aqueous solutions and liquid metals in packed bed", Chem. Eng. Sci., 23, 945 (1968).

APPENDIX I

Derivation of the Equation of Surface Area of Mass Transfer for Benzoic Acid:

Consider a coated particle as shown in Figure 16 having a surface area A_p. The density of the coating material is ρ. ρ_B and ρ_D are the densities of the benzoic acid and the dye respectively.

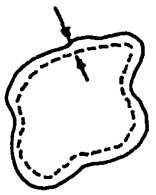

Figure 16. A differential element on particle surface

For an element of the surface having a thickness of d, the weight of the element can be expressed as:

$$\rho A_p \Delta d = \Delta M_B + \Delta M_D, \qquad \text{(I)}$$

where ΔM_B and ΔM_D are the weight of the benzoic acid and the dye in the element respectively. If the ratio of benzoic acid to dye is r, i.e. $\frac{\Delta M_B}{\Delta M_D}$, and the coating material is uniform, then

$$\rho A_p \Delta d = \Delta M_B + \frac{\Delta M_B}{r}$$

$$= \Delta M_B (1+\frac{1}{r}). \qquad \text{(II)}$$

If Δd approaches zero, then

$$\rho A_p \Delta d = \rho_B A \Delta d \ (1+\frac{1}{r}), \qquad \text{(III)}$$

where A is the surface area of benzoic acid on the particle

surface. Then,

$$A = \frac{\rho A_P}{\rho_B (1+1/r)} \qquad \text{(IV)}$$

if r is large; hence $\rho = \rho_B$

Eq. (IV) can be rewritten as:

$$A = A_P \left(\frac{r}{1 + r}\right) \qquad \text{(V)}$$

APPENDIX II

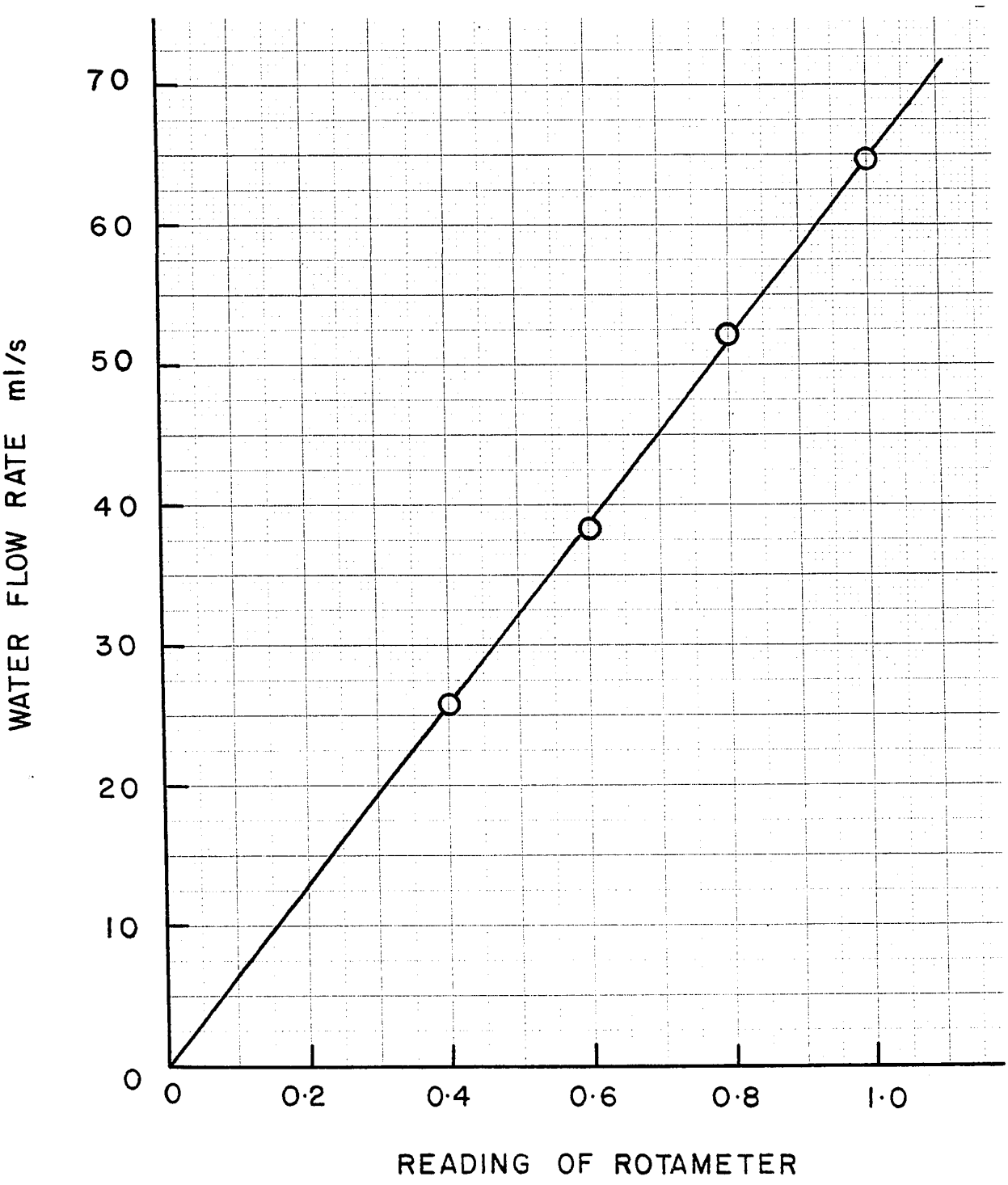

Figure 17. Calibration Curve of Liquid Rotameter (I)

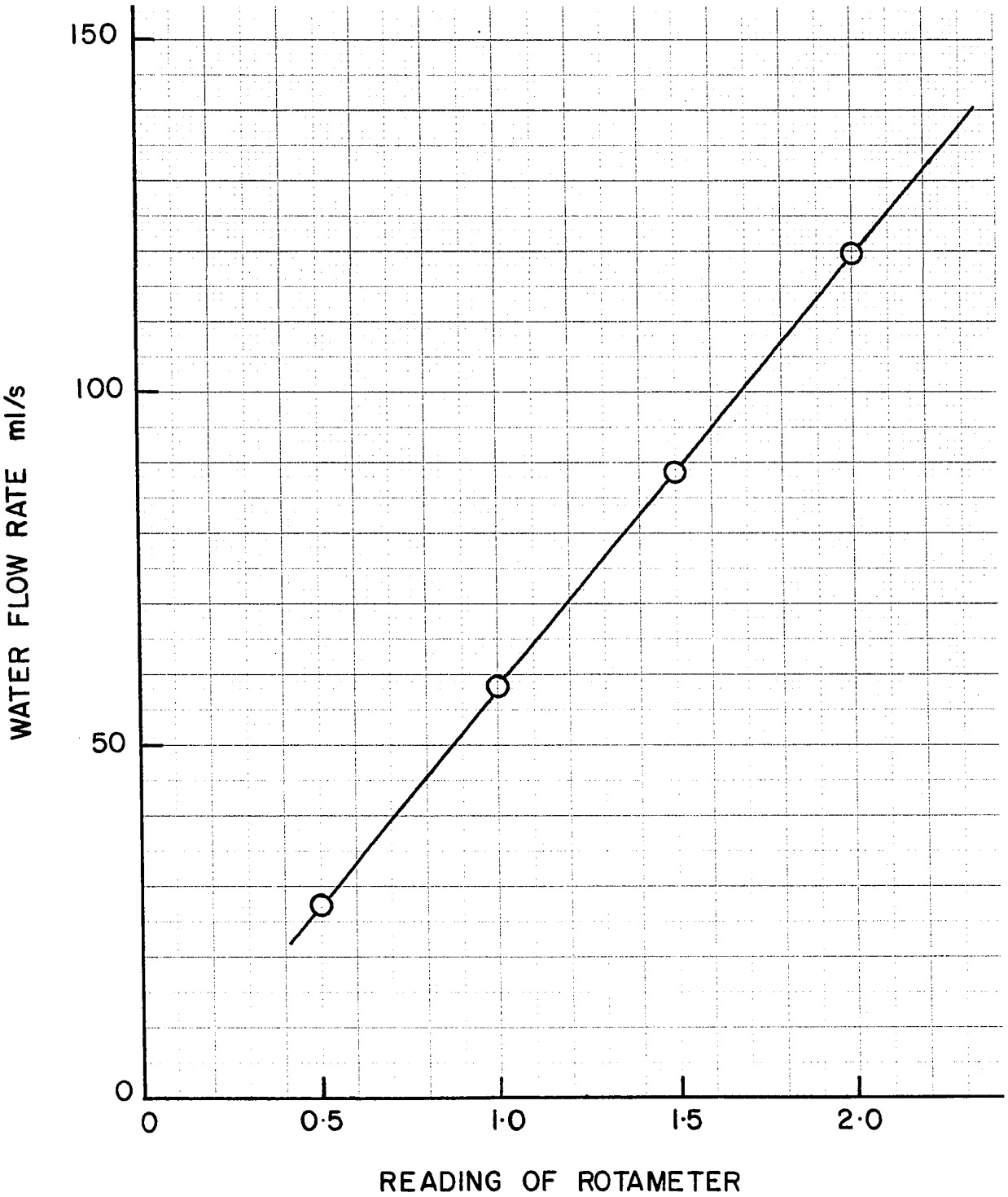

Figure 18. Calibration Curve of Liquid Rotameter (II)

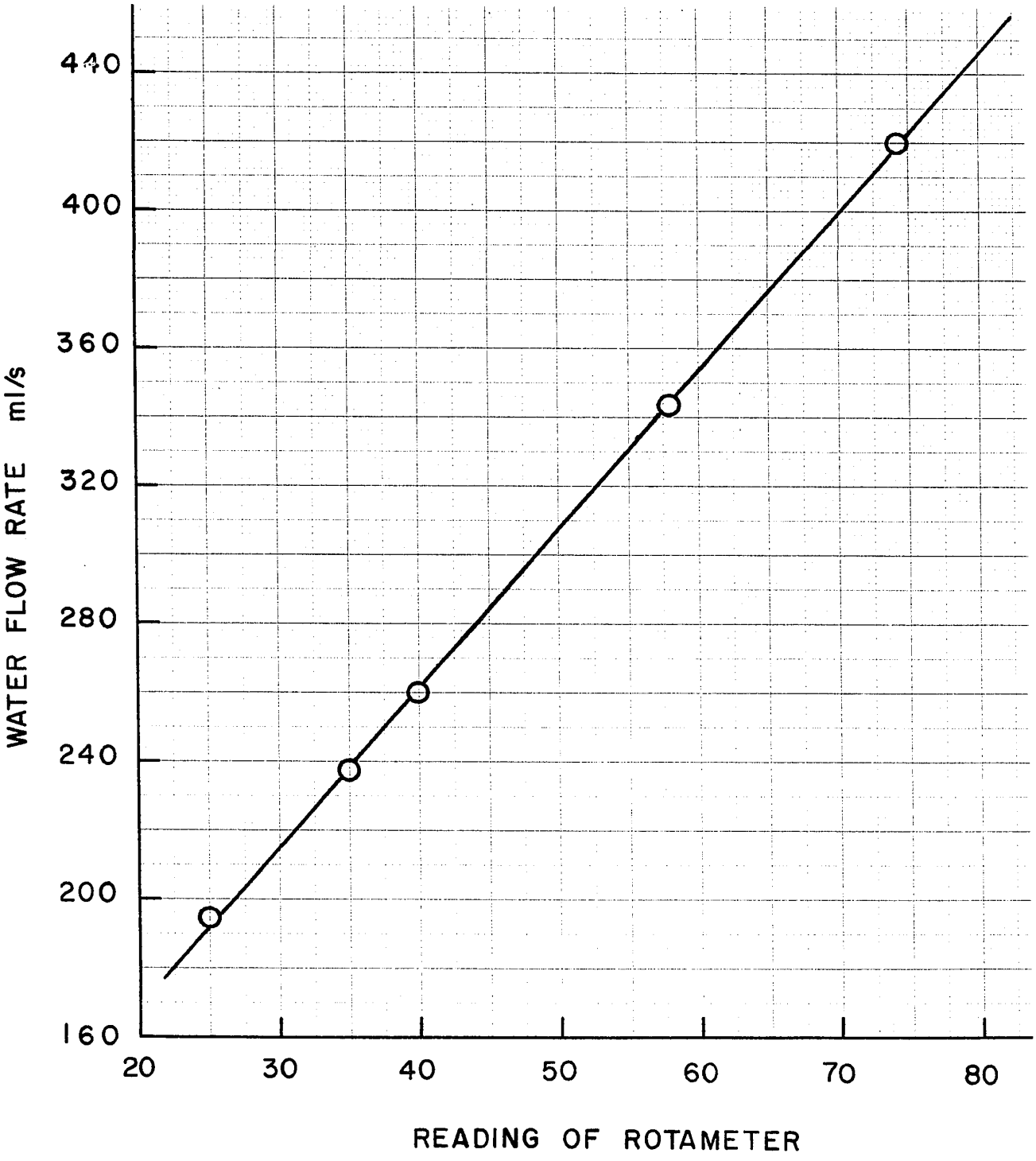

Figure 19. Calibration Curve of Liquid Rotameter (IV)

Rotameter Reading	Upstream Pressure in Orifice (atm)	Pressure Drop $*10^2$ (atm)	Gas flow Rate $*10^3$ kg/sec
2	2.63	0.79	1.47
4	2.63	3.50	3.08
6	2.63	7.87	4.59
10	2.63	21.81	7.65

Table 6. Calibration of Gas Rotameter

APPENDIX III

```
$JOB  ACCT-NUM,'C.S.YANG',PAGE=30,TIME=20
C*****************************************************************************
C
C      COMPUTER PROGRAM
C
C      ***********************************
C      *                                 *
C      *     PART 1.  NOMENCLATURE       *
C      *                                 *
C      ***********************************
C
C
C      AP     :  PARTICLE SURFACE AREA.
C
C      AS     :  PARTICLE EXTERNAL AREA PER UNIT VOLUME OF THE TEST PART.
C
C      C1     :  CONCENTRATION OF BENZOIC ACID AT OUTLET.
C
C      CS     :  SOLUBILITY OF BENZOIC ACID IN WATER.
C
C      D      :  DIFFUSIVITY.
C
C      DEN    :  DENSITY OF LIQUID.
C
C      DP     :  EFFECTIVE PARTICLE DIAMETER.
C
C      DPLG   :  PRESSURE GRADIENT.
C
C      E      :  POROSITY.
C
C      ELM    :  POWER DISSIPATION PER UNIT MASS OF LIQUID HOLDUP.
C
C      G      :  GAS MASS FLOW RATE.
C
C      JD     :  MASS TRANSFER FACTOR.
C
C      K      :  MASS TRANSFER COEFFICIENT.
C
C      KO     :  KOLMOGOROFF NUMBER.
C
C      L      :  LIQUID MASS FLOW RATE.
C
C      R      :  READING OF GAS ROTAMETER.
C
C      RE     :  LIQUID REYNOLDS NUMBER.
C
C      REM    :  MODIFIED LIQUID REYNOLDS NUMBER.
C
C      SC     :  SCHMIDT NUMBER.
C
C      SH     :  SHERWOOD NUMBER.
C
C      SHM    :  MODIFIED SHERWOOD NUMBER.
C
C      T      :  LIQUID TEMPERATURE.
C
C      VIS    :  LIQUID VISCOSITY.
C
C*****************************************************************************
```

```
C*******************************************************************************
C
C
C     ************************************
C     *                                  *
C     *     PART 2.  MAIN PROGRAM        *
C     *                                  *
C     ************************************
C
C
      DIMENSION EEL(35),AJD(35)
      DIMENSION VL(35),YM(35)
      DIMENSION SCK(35),CS(35)
      DIMENSION D(35),DEN(35),VIS(35),SH(35),SC(35),Y(35),RE(35)
      DIMENSION L(35),E(35),C(35),C1(35),A(20),T(35),K(35)
      DIMENSION SHM(35),DPLG(35),G(35),R(35) ,HOLDUP(35),TG(35),YY(35)
      DIMENSION ELM(35),REM(35)
      REAL KO(35)
      REAL K,L
      REAL KSOL
C
C
C     CALCULATION OF PHYSICAL PROPERTIES OF FLUIDS, REYNOLDS NUMBERS,
C     MASS TRANSFER COEFFICIENTS, SCHMIDT NUMBERS AND SHERWOOD NUMBERS.
C
C
      S=44.696E-04
      AS=899
      DP=0.847*0.01
      READ,(R(I),I=1,35)
      READ,(CI(I),I=1,35)
   31 FORMAT('1',' ')
      AP=2.25E-04
      READ,(DPLG(I),I=1,35)
      READ,(TG(I),I=1,35)
      PRINT87
      NNN=35
      READ3,(L(I),T(I),E(I),C(I),I=1,NNN)
    3 FORMAT(4F10.5)
      PRINT,' '
      PRINT,' '
      PRINT63
   63 FORMAT(6X,'RUN',4X,'TEMPERATURE',3X,'DENSITY',6X,'VISCOSITY',3X,
     $'DIFFUSIVITY',3X,'POROSITY'/)
      PRINT,  '                                                    3
     $  9'
      PRINT,  '                                                 * 10           *
     $10'
      PRINT94
   94 FORMAT(/16X,'0',15X,'3',24X,'2')
      PRINT96
   96 FORMAT(17X,'C',10X,'KG/M',9X,'KG/M.S',9X,'M /S'/)
      DO 8 I=1,NNN
      DPLG(I)=DPLG(I)*10
      L(I)=L(I)*1.0E-06
      VIS(I)=0.140018E-01-0.202656E-03*T(I)
      VIS(I)=VIS(I)*0.1
      DEN(I)=0.100342E 01-0.259399E-03*T(I)
C
C
```

```
      C
      C
      C
      C
   40         DEN(I)=DEN(I)*1000
   41         D(I)=1.000E-05*(0.8937*.001/VIS(I))**1.14
   42         D(I)=D(I)*0.0001
   43         CS(I)=1.7+0.0197*T(I)+0.0020*T(I)*T(I)
   44         VL(I)=L(I)/S
   45         L(I)=L(I)*DEN(I)/S
   46         SC(I)=VIS(I)/(DEN(I)*D(I))
   47         B=C1(I)/CS(I)
   48         K(I)=(VL(I)*S/(150*AP))*ALOG(1/(1-B))
   49         SH(I)=DP*K(I)/D(I)
   50         Y(I)=E(I)*SH(I)*(SC(I)**(-0.33333))
   51         RE(I)=VL(I)*DEN(I)*DP/VIS(I)
   52         W=(-0.131729+0.803676*R(I))*0.001
   53         G(I)=(W/S)*SQRT(535./(TG(I)+460))
   54         TG(I)=(TG(I)-32)*(5./9.)
   55         IF(I.EQ.7.OR.I.EQ.14.OR.I.EQ.19.OR.I.EQ.26.OR.I.EQ.32) PRINT79
   56      79 FORMAT(' ')
   57         VISCOS=VIS(I)*1000
   58         DIFF=D(I)*1.00E 09
   59         PRINT66,I,T(I),DEN(I),VISCOS,DIFF,E(I)
   60      66 FORMAT(' ',5X,I2,5(5X,F8.3))
   61       8 CONTINUE
   62         PRINT80
   63      80 FORMAT(//)
   64         PRINT,'       TABLE  7.  EXPERIMENTAL DATA (I).'
   65         PRINT87
   66         PRINT,' '
   67         PRINT64
   68      64 FORMAT(///6X,'RUN',9X,'L',12X,'G',11X,'CS',12X,'C1',10X,'SC')
   69         PRINT68
   70      68 FORMAT(19X,'2',12X,'2')
   71         PRINT67
   72      67 FORMAT(15X,'KG/M.S',7X,'KG/M.S',9X,'G/L',10X,'G/L'/)
   73         DO 41 I=1,NNN
   74         IF(I.EQ.7.OR.I.EQ.13.OR.I.EQ.18.OR.I.EQ.25.OR.I.EQ.31) PRINT79
   75         PRINT62,I,L(I),G(I),CS(I),C1(I),SC(I)
   76      62 FORMAT(' ',5X,I2,5(5X,F8.3))
   77      41 CONTINUE
   78         PRINT80
   79         PRINT,'       TABLE  8.  EXPERIMENTAL DATA (II)'
   80         PRINT87
   81      87 FORMAT('1')
   82         PRINT55
   83      55 FORMAT (///6X,'RUN',09X,'L',13X,'G',12X,'K',12X,'RE',6X,'E*SH/SC**
     $(1/3)'/)
   84         PRINT,'                                                    5'
   85         PRINT,'                                                * 10'
   86         PRINT,' '
   87         PRINT34
   88      34 FORMAT(20X,'2',11X,'2')
   89         PRINT37
   90      37 FORMAT(16X,'KG/M.S',6X,'KG/M.S',10X,'M/S'/)
      C
      C
      C
      C
```

```
      C
      C
      C
   91       DO 72 I=1,NNN
   92       LRUN=I
   93       IF(I.EQ.7.OR.I.EQ.13.OR.I.EQ.18.OR.I.EQ.25.OR.I.EQ.31) PRINT79
   94       KSCL=K(I)*1.0 E 05
   95       PRINT78,LRUN,L(I),G(I),KSCL,RE(I),Y(I)
   96    78 FORMAT(' ',5X,I2,5X,F8.2,5X,F8.3,5X,F9.3,5X,F8.2,5X,F8.2)
   97    72 CONTINUE
   98       PRINT80
   99       PRINT,'      TABLE  9.  COMPUTED VARIABLES DERIVED FROM THE EXPERI
           $MENTAL MEASUREMENTS (III)'
  100       PRINT,' '
      C
      C
      C     CALCULATION OF LIQUID HOLDUP EY USING SPECCHIA'S EQUATION.
      C
      C
  101       DO 801 I=1,NNN
  102       DN=0.25*2.54*0.01
  103       GA   =(DN **3)*DEN(I)*(DEN(I)*9.8+DPLG(I))/(VIS(I)**2)
  104       GRE=G(I)*DN/1.8E-05
  105       RENYL=L(I)*DN/VIS(I)
  106       Z=GRE**1.167/(RENYL**0.767)
  107       IF(L(I).GE.10.0.OR.G(I).GE.9.15) THEN DO
  108       HOLDUP(I)=0.125*( Z   **(-0.312))*((AS*DN/E(I))**0.65)
  109       ELSE DO
  110       HOLDUP(I)=3.86*(RENYL**0.545)*(GA    **(-0.42))*(DN*AS/E(I))**0.65
  111       END IF
  112       HOLDUP(I)=HOLDUP(I)*E(I)
  113       HOLDUP(I)=HOLDUP(I)+0.0823
      C
      C
      C     CALCULATION OF KOLMOGOROFF NUMBERS, POWER DISSIPATIONS,
      C     MASS TRANSFER FACTORS, MODIFIED SHERWOOD NUMBERS AND
      C     MODIFIED REYNOLDS NUMBERS.
      C
      C
  114       SHM(I)=K(I)/(D(I)*AS)
  115       YM(I)=E(I)*SHM(I)/(SC(I)**0.333333333)
  116       EEL(I)=(DPLG(I)*VL(I)*VIS(I))/(HOLDUP(I)*(DEN(I)**2))
  117       ELM(I)=DPLG(I)*VL(I)/(HOLDUP(I)*DEN(I))
  118       KO(I)=     (ELM(I)*(DP **4)*(DEN(I)**3)/(VIS(I)**3))
  119       YY(I)=     ((K(I)*DP /D(I))*(SC(I)**(-.33333)))
  120       REM(I)=VL(I)*DEN(I)/(HOLDUP(I)*VIS(I)*AS)
  121       SCK(I)=K(I)*(SC(I)**.666666666)
  122       AJD(I)=(K(I)/VL(I))*(VIS(I)/(DEN(I)*D(I)))**0.6666666
  123    801 CONTINUE
  124       PRINT87
  125       PRINT,' '
  126       PRINT,' '
  127       PRINT,' '
  128       PRINT56
  129    56 FORMAT(6X,'RUN',09X,'L',12X,'G',11X,'REM',6X,'E*SHM/SC**(1/3)',3X,
           $'RE',11X,'JD'/)
  130       PRINT,' '
  131       PRINT35
      C
      C
```

```
      C
      C
      C
      C
  132     35 FORMAT(20X,'2',11X,'2')
  133        PRINT32
  134     32 FORMAT(16X,'KG/M.S',6X,'KG/M.S')
  135        PRINT,' '
  136        DO 39 I=1,35
  137        LRUN=I
  138        IF(I.EQ.7.OR.I.EQ.13.OR.I.EQ.18.OR.I.EQ.25.OR.I.EQ.31) PRINT79
  139        PRINT65,I,L(I),G(I),REM(I),YM(I),RE(I),AJD(I)
  140     65 FORMAT(' ',5X,I2,5X,F8.2,5X,F8.3,5X,F8.1,5X,F8.2,5X,F8.1,5X,F8.3)
  141     39 CONTINUE
  142        PRINT80
  143        PRINT,'      TABLE 10.  COMPUTED VARIABLES DERIVED FROM THE EXPERI
             $MENTAL MEASUREMENTS (II)'
  144        PRINT31
  145        PRINT57
  146     57 FORMAT(///6X,'RNN',9X,'L',12X,'G',10X,'DPLG',09X,'HOLDUP',5X,'ELM*
             $VIS/DEN',3X,'K*SC**(2/3)'/)
  147        PRINT,  '
             $                7                3'
  148        PRINT,  '
             $           * 10             * 10'
  149        PRINT,' '
  150        PRINT36
  151     36 FORMAT(20X,'2',12X,'2',11X,'3',24X,'4',2X,'4')
  152        PRINT33
  153     33 FORMAT(16X,'KG/M.S',7X,'KG/M.S',7X,'N/M',24X,'M /S',11X,'M/S')
  154        PRINT,' '
  155        DO 38 I=1,35
  156        IF(I.EQ.7.OR.I.EQ.13.OR.I.EQ.18.OR.I.EQ.25.OR.I.EQ.31) PRINT79
  157        SCKSOL=SCK(I)*1.0E 03
  158        EELDIS=EEL(I)*1.0E 07
  159        PRINT61,I,L(I),G(I),DPLG(I),HOLDUP(I),EELDIS,SCKSOL
  160     61 FORMAT(' ',5X,I2,5X,F8.2,5X,F8.3,5X,F8.1,5X,F8.3,5X,F9.3,5X,F9.3)
  161     38 CONTINUE
  162        PRINT80
  163        PRINT,'      TABLE 11.  COMPUTED VARIABLES DERIVED FROM THE EXPERI
             $MENTAL MEASUREMENTS (III).     '
      C
      C
      C     CORRELATION OF RESULTS BY USING LEAST-SQUARES METHOD.
      C
      C
  164        CALL CURVE(35,0.1,RE,AJD)
  165        CALL CURVE(19,16.2,EEL,SCK)
  166        CALL CURVE(19,16.3,KO,YY)
  167        CALL CURVE(14,0.4,REM,YM)
  168        CALL CURVE(6,12,4,REM,YM)
  169        CALL CURVE(18,17,4,REM,YM)
  170        PRINT87
  171        STOP
  172        END
      C
      C
      C
      C
      C
```

```
C
C*******************************************************************************
C*******************************************************************************
C
C
C      ************************************
C      *                                  *
C      *      PART 3.  SUBROUTINES        *
C      *                                  *
C      ************************************
C
C
      SUBROUTINE CURVE(NN,NC,N ,XC,YC)
C
      DIMENSION A(20)
      DIMENSION XO(35),YO(35),XLOG(35),YLOG(35)
      CHARACTER*16 NUMBER(5),NAME(5)
      NUMBER(5)='        Y         '
      NUMBER(1)='       JD         '
      NUMBER(3)=' SH/SC**(1/3)     '
      NUMBER(2)='  K*SC**(2/3)     '
      NUMBER(4)='E*SHM/SC**(1/3)   '
      NAME(5)='         G         '
      NAME(1)='        RE         '
      NAME(2)='  (ELM*VIS/DEN)    '
      NAME(3)='        KO         '
      NAME(4)='       REM         '
      PRINT87
   87 FORMAT('1')
      PRINT,' '
      PRINT,' '
      PRINT12
   12 FORMAT(//////)
      PRINT,'                  RUN           ',NAME(N)     ,'       ',NUMBER(N)
     $)
      PRINT,' '
      PRINT,' '
      DO 10 I=1,NN
      J=I+NO
      YLOG(I)=ALOG(YO(J))/2.303
      XLOG(I)=ALOG(XO(J))/2.303
      PRINT14,J,XO(J),YO(J)
   14 FORMAT(16X,I2,12X,E13.7,12X,E13.7)
   10 CONTINUE
      PRINT,' '
      PRINT,' '
      PRINT,'                A LEAST-SQUARES FIT OF THE ABOVE DATA IS GIVE
     $N BY :'
      CALL LESQ(NN,1,A,XLOG,YLOG)
      A(1)=10**(A(1))
      PRINT15,A(2)
   15 FORMAT(///65X,F6.3)
      PRINT,' '
      PRINT,'          ',NUMBER(N),'=',A(1),' ',NAME(N)
      RETURN
      END
C
C
C
```

```
C
C
C
C
C*************************************************************************
C*************************************************************************
      SUBROUTINE LESQ(NN,M,A,X,Y)
C
      DIMENSION X( 35),Y( 35),XC(35),YX(20),E(20),A(20),B(20),C(20,20),D
     $(20,20)
      N=NN-1
      NP1=N+1
      MP1=1+M
      M2=M*2
      DO 20 K=1,M2
      XC(K)=0.0
      DO 15 I=1,NP1
   15 XC(K)=XC(K)+X(I)**K
   20 CONTINUE
      YC=0.0
      DO 22 I=1,NP1
   22 YC=YC+Y(I)
      DO 30 K=1,M
      YX(K)=0.0
      DO 25 I=1,NP1
   25 YX(K)=YX(K) +Y(I)*X(I)**K
   30 CONTINUE
      DO 40 I=1,MP1
      DO 35 J=1,MP1
      IPJM2=I+J-2
      IF(IPJM2)33,31,33
   31 C(1,1)=FLOAT(NP1)
      GO TO 35
   33 C(I,J)=XC(IPJM2)
   35 CONTINUE
   40 CONTINUE
      B(1)=YC
      DO 45 I=2,MP1
   45 B(I)=YX(I-1)
      CALL INVERS (C,D,MP1)
      DO 55 I=1,MP1
      A(I)=0.0
      DO 54 J=1,MP1
   54 A(I)=A(I)+D(I,J)*B(J)
   55 CONTINUE
      OO=1
      IF(OO.GE.0) GO TO 99
      WRITE(6,111)
      WRITE(6,110) (A(K),K=1,MP1)
  110 FORMAT(1X,E14.6)
  111 FORMAT(18H COEFFICIENTS A(K))
   99 CONTINUE
      RETURN
      END
C
C
C
C
```

```
C
C
C
C
C
      SUBROUTINE INVERS (A,B,N)
C
      DIMENSION A(20,20),B(20,20)
      EPS=0.0000001
      DO 6 I=1,N
      DO 5 J=1,N
      IF(I-J)4,3,4
    3 B(I,J)=1.0
      GO TO 5
    4 B(I,J)=0
    5 CONTINUE
    6 CONTINUE
      DEL=1.0
      DO 45 K=1,N
      IF((K-N).GE.0.0) GO TO 30
   12 IMAX=K
      AMAX=ABS(A(K,K))
      KP1=K+1
      DO 20 I=KP1,N
      IF(AMAX-ABS(A(I,K))) 15,20,20
   15 IMAX=I
      AMAX=ABS(A(I,K))
   20 CONTINUE
      IF(IMAX-K)25,30,25
   25 DO 29 J=1,N
      ATMP=A(IMAX,J)
      A(IMAX,J)=A(K,J)
      A(K,J)=ATMP
      BTMP=B(IMAX,J)
      B(IMAX,J)=B(K,J)
   29 B(K,J)=BTMP
      DEL=-DEL
   30 CONTINUE
      IF(ABS(A(K,K))-EPS)93,93,35
   35 DEL=A(K,K)*DEL
      DIV=A(K,K)
      DO 38 J=1,N
      A(K,J)=A(K,J)/DIV
   38 B(K,J)=B(K,J)/DIV
      DO 43 I=1,N
      AMULT=A(I,K)
      IF(I-K)39,43,39
   39 DO 42 J=1,N
      A(I,J)=A(I,J)-AMULT*A(K,J)
   42 B(I,J)=B(I,J)-AMULT*B(K,J)
   43 CONTINUE
   45 CONTINUE
      OO=1
      IF(OO.GE.0) GO TO 99
      WRITE(6,120)
      WRITE(6,110) ((B(I,J),I=1,N),J=1,N)
      WRITE(6,121)
C
C
```

```
C
C
C
311         WRITE(6,110) DEL
312      93 WRITE(6,113) K
313         GO TO 99
314     110 FORMAT(2X,E15.8)
315     113 FORMAT(25H SINGULAR MATRIX FOR K = ,I2)
316     120 FORMAT (20H ELEMENTS OF INVERSE)
317     121 FORMAT(21H VALUE OF DETERMINANT)
318      99 RETURN
319         END

$ENTRY
```

RUN	TEMPERATURE	DENSITY	VISCOSITY	DIFFUSIVITY	POROSITY
			$* 10^{3}$	$* 10^{9}$	
	^{0}C	KG/M^{3}	KG/M.S	M^{2}/S	
1	24.300	997.116	0.908	0.982	0.606
2	24.200	997.142	0.910	0.980	0.602
3	24.200	997.142	0.910	0.980	0.602
4	24.200	997.142	0.910	0.980	0.595
5	24.300	997.116	0.908	0.982	0.611
6	24.800	996.987	0.898	0.995	0.595
7	25.000	996.935	0.894	1.000	0.624
8	25.000	996.935	0.894	1.000	0.624
9	24.800	996.987	0.898	0.995	0.618
10	24.300	997.116	0.908	0.982	0.604
11	24.800	996.987	0.898	0.995	0.618
12	24.400	997.091	0.906	0.985	0.608
13	24.600	997.039	0.902	0.990	0.602
14	24.900	996.961	0.896	0.998	0.614
15	24.800	996.987	0.898	0.995	0.620
16	24.900	996.961	0.896	0.998	0.602
17	24.000	997.194	0.914	0.975	0.594
18	25.200	996.883	0.889	1.005	0.622
19	25.100	996.909	0.892	1.003	0.606
20	25.000	996.935	0.894	1.000	0.605
21	24.800	996.987	0.898	0.995	0.591
22	24.800	996.987	0.898	0.995	0.606
23	24.900	996.961	0.896	0.998	0.624
24	24.300	997.116	0.908	0.982	0.613
25	24.200	997.142	0.910	0.980	0.608
26	24.200	997.142	0.910	0.980	0.611
27	24.300	997.116	0.908	0.982	0.600
28	23.400	997.350	0.926	0.960	0.608
29	24.500	997.064	0.904	0.987	0.626
30	24.400	997.091	0.906	0.985	0.593
31	25.100	996.909	0.892	1.003	0.605
32	24.300	997.116	0.908	0.982	0.596
33	24.400	997.091	0.906	0.985	0.607
34	24.600	997.039	0.902	0.990	0.636
35	24.300	997.116	0.908	0.982	0.611

TABLE 7. EXPERIMENTAL DATA (I).

RUN	L $KG/M^2.S$	G $KG/M^2.S$	CS G/L	C1 G/L	SC
1	2.097	0.330	3.360	0.111	926.657
2	2.097	0.687	3.348	0.117	931.066
3	2.097	1.045	3.348	0.131	931.066
4	2.097	1.049	3.348	0.126	931.066
5	2.097	1.770	3.360	0.133	926.657
6	2.097	1.769	3.419	0.129	904.780
7	4.260	0.330	3.442	0.085	896.106
8	4.260	0.688	3.442	0.084	896.106
9	4.260	1.047	3.419	0.087	904.780
10	4.261	1.048	3.360	0.106	926.657
11	4.260	1.767	3.419	0.096	904.780
12	4.261	1.769	3.371	0.103	922.260
13	10.596	0.331	3.395	0.061	913.498
14	10.595	0.330	3.431	0.061	900.438
15	10.595	0.690	3.419	0.082	904.780
16	10.595	1.047	3.431	0.101	900.438
17	10.598	1.767	3.325	0.108	939.917
18	21.411	0.330	3.467	0.072	887.476
19	21.189	0.688	3.454	0.081	891.786
20	21.190	1.047	3.442	0.091	896.106
21	21.191	1.052	3.419	0.089	904.780
22	21.191	1.769	3.419	0.101	904.780
23	21.190	1.767	3.431	0.091	900.438
24	21.193	1.772	3.360	0.088	926.657
25	52.985	0.330	3.348	0.041	931.066
26	52.985	0.690	3.348	0.045	931.066
27	52.984	1.051	3.360	0.048	926.657
28	52.996	1.050	3.256	0.043	966.735
29	52.981	1.770	3.383	0.052	917.874
30	52.692	1.769	3.371	0.049	922.260
31	97.648	0.331	3.454	0.029	891.786
32	95.259	0.690	3.360	0.029	926.657
33	94.096	1.051	3.371	0.031	922.260
34	93.690	1.770	3.395	0.034	913.498
35	92.091	1.769	3.360	0.037	926.657

TABLE 8. EXPERIMENTAL DATA (II)

RUN	L	G	K	RE	E*SH/SC**(1/3)
			* 10^5		
	$KG/M^2.S$	$KG/M^2.S$	M/S		
1	2.10	0.330	0.935	19.57	5.02
2	2.10	0.687	0.988	19.52	5.27
3	2.10	1.045	1.113	19.52	5.93
4	2.10	1.049	1.066	19.52	5.61
5	2.10	1.770	1.123	19.57	6.07
6	2.10	1.769	1.071	19.79	5.61
7	4.26	0.330	1.420	40.38	7.79
8	4.26	0.688	1.404	40.38	7.79
9	4.26	1.047	1.455	40.20	7.91
10	4.26	1.048	1.819	39.76	9.71
11	4.26	1.767	1.611	40.20	8.76
12	4.26	1.769	1.764	39.85	9.47
13	10.60	0.331	2.550	99.54	13.53
14	10.60	0.330	2.513	100.20	13.57
15	10.60	0.690	3.416	99.98	18.63
16	10.60	1.047	4.197	100.20	22.20
17	10.60	1.767	4.628	98.23	24.37
18	21.41	0.330	5.983	203.89	32.65
19	21.19	0.688	6.713	201.31	35.68
20	21.19	1.047	7.548	200.86	40.11
21	21.19	1.052	7.409	199.96	38.52
22	21.19	1.769	8.467	199.96	45.13
23	21.19	1.767	7.590	200.41	41.66
24	21.19	1.772	7.489	197.76	40.58
25	52.98	0.330	8.752	493.30	47.12
26	52.98	0.690	9.548	493.30	51.65
27	52.98	1.051	10.198	494.39	54.09
28	53.00	1.050	9.329	484.76	50.63
29	52.98	1.770	10.940	496.58	60.48
30	52.69	1.769	10.240	492.77	53.67
31	97.65	0.331	10.758	927.72	57.15
32	95.26	0.690	10.857	888.86	57.25
33	94.10	1.051	11.716	879.98	62.85
34	93.69	1.770	12.551	880.11	70.34
35	92.09	1.769	13.658	859.30	73.81

TABLE 9. COMPUTED VARIABLES DERIVED FROM THE EXPERIMENTAL MEASUREMENTS (III)

RUN	L	G	REM	E*SHM/SC**(1/3)	RE	JD
	$KG/M^2.S$	$KG/M^2.S$				
1	2.10	0.330	15.9	0.66	19.6	0.423
2	2.10	0.687	16.3	0.69	19.5	0.448
3	2.10	1.045	16.7	0.78	19.5	0.505
4	2.10	1.049	16.8	0.74	19.5	0.483
5	2.10	1.770	17.5	0.80	19.6	0.508
6	2.10	1.769	17.8	0.74	19.8	0.477
7	4.26	0.330	26.8	1.02	40.4	0.309
8	4.26	0.688	27.6	1.01	40.4	0.305
9	4.26	1.047	28.5	1.04	40.2	0.319
10	4.26	1.048	28.3	1.28	39.8	0.405
11	4.26	1.767	30.2	1.15	40.2	0.353
12	4.26	1.769	30.0	1.24	39.8	0.391
13	10.60	0.331	53.7	1.78	99.5	0.226
14	10.60	0.330	53.7	1.78	100.2	0.221
15	10.60	0.690	63.4	2.45	100.0	0.301
16	10.60	1.047	69.9	2.92	100.2	0.368
17	10.60	1.767	76.3	3.20	98.2	0.418
18	21.41	0.330	97.0	4.29	203.9	0.257
19	21.19	0.688	115.6	4.69	201.3	0.293
20	21.19	1.047	127.0	5.27	200.9	0.330
21	21.19	1.052	127.2	5.06	200.0	0.326
22	21.19	1.769	141.3	5.93	200.0	0.373
23	21.19	1.767	140.7	5.47	200.4	0.333
24	21.19	1.772	139.6	5.33	197.8	0.335
25	52.98	0.330	202.6	6.19	493.3	0.157
26	52.98	0.690	245.3	6.78	493.3	0.171
27	52.98	1.051	273.6	7.10	494.4	0.182
28	53.00	1.050	268.2	6.65	484.8	0.172
29	52.98	1.770	306.8	7.94	496.6	0.194
30	52.69	1.769	308.3	7.05	492.8	0.184
31	97.65	0.331	340.6	7.51	927.7	0.102
32	95.26	0.690	402.9	7.52	888.9	0.108
33	94.10	1.051	442.9	8.25	880.0	0.118
34	93.69	1.770	497.2	9.24	880.1	0.126
35	92.09	1.769	491.4	9.69	859.3	0.141

TABLE 10. COMPUTED VARIABLES DERIVED FROM THE EXPERIMENTAL MEASUREMENTS (II)

RNN	L	G	DPLG	HOLDUP	ELM*VIS/DEN	K*SC**(2/3)
					$* 10^{7}$	$* 10^{3}$
	$KG/M^2.S$	$KG/M^2.S$	N/M^3		M^4/S^4	M/S
1	2.10	0.330	1070.0	0.161	0.127	0.889
2	2.10	0.687	2230.0	0.158	0.272	0.942
3	2.10	1.045	4090.0	0.153	0.513	1.061
4	2.10	1.049	4090.0	0.153	0.514	1.016
5	2.10	1.770	7860.0	0.147	1.028	1.068
6	2.10	1.769	7860.0	0.146	1.023	1.002
7	4.26	0.330	1310.0	0.198	0.254	1.320
8	4.26	0.688	2840.0	0.192	0.569	1.305
9	4.26	1.047	4840.0	0.185	1.009	1.361
10	4.26	1.048	4840.0	0.185	1.023	1.729
11	4.26	1.767	9040.0	0.175	1.997	1.507
12	4.26	1.769	9040.0	0.174	2.018	1.671
13	10.60	0.331	2080.0	0.243	0.824	2.401
14	10.60	0.330	2080.0	0.245	0.813	2.344
15	10.60	0.690	4250.0	0.207	1.971	3.195
16	10.60	1.047	6770.0	0.188	3.442	3.914
17	10.60	1.767	11440.0	0.169	6.606	4.441
18	21.41	0.330	4670.0	0.276	3.252	5.526
19	21.19	0.688	8120.0	0.229	6.771	6.219
20	21.19	1.047	11360.0	0.208	10.448	7.016
21	21.19	1.052	11360.0	0.206	10.565	6.931
22	21.19	1.769	15010.0	0.186	15.497	7.920
23	21.19	1.767	15010.0	0.187	15.364	7.077
24	21.19	1.772	15010.0	0.186	15.661	7.118
25	52.98	0.330	16150.0	0.320	24.555	8.345
26	52.98	0.690	22250.0	0.264	40.967	9.104
27	52.98	1.051	25800.0	0.237	52.753	9.693
28	53.00	1.050	25800.0	0.237	53.763	9.121
29	52.98	1.770	29830.0	0.213	67.776	10.333
30	52.69	1.769	29830.0	0.210	68.405	9.702
31	97.65	0.331	34000.0	0.358	83.522	9.967
32	95.26	0.690	36600.0	0.290	110.193	10.320
33	94.10	1.051	39790.0	0.261	131.086	11.101
34	93.69	1.770	42860.0	0.232	157.136	11.816
35	92.09	1.769	42860.0	0.230	157.384	12.982

TABLE 11. COMPUTED VARIABLES DERIVED FROM THE EXPERIMENTAL MEASUREMENTS (III).

RUN	RE	JD
1	0.1956741E 02	0.4226652E 00
2	0.1952432E 02	0.4479588E 00
3	0.1952432E 02	0.5045510E 00
4	0.1952432E 02	0.4832194E 00
5	0.1956741E 02	0.5076042E 00
6	0.1978572E 02	0.4765597E 00
7	0.4038315E 02	0.3089486E 00
8	0.4038315E 02	0.3052847E 00
9	0.4020288E 02	0.3185640E 00
10	0.3975928E 02	0.4046250E 00
11	0.4020288E 02	0.3527499E 00
12	0.3984721E 02	0.3910779E 00
13	0.9953685E 02	0.2259053E 00
14	0.1002047E 03	0.2205198E 00
15	0.9998106E 02	0.3006571E 00
16	0.1002047E 03	0.3682866E 00
17	0.9822771E 02	0.4178488E 00
18	0.2038874E 03	0.2572682E 00
19	0.2013101E 03	0.2926084E 00
20	0.2008587E 03	0.3300866E 00
21	0.1999621E 03	0.3260809E 00
22	0.1999621E 03	0.3726342E 00
23	0.2004094E 03	0.3329837E 00
24	0.1977557E 03	0.3349056E 00
25	0.4933010E 03	0.1570404E 00
26	0.4933010E 03	0.1713285E 00
27	0.4943894E 03	0.1824231E 00
28	0.4847646E 03	0.1716439E 00
29	0.4965811E 03	0.1944526E 00
30	0.4927708E 03	0.1835909E 00
31	0.9277214E 03	0.1017528E 00
32	0.8888599E 03	0.1080189E 00
33	0.8799778E 03	0.1176270E 00
34	0.8801145E 03	0.1257477E 00
35	0.8593010E 03	0.1405640E 00

A LEAST-SQUARES FIT OF THE ABOVE DATA IS GIVEN BY :

$$JD = 0.1254092E\ 01 \times RE^{-0.315}$$

RUN	(ELM*VIS/DEN)	K*SC**(2/3)
17	0.6605941E-06	0.4440628E-02
18	0.3252067E-06	0.5525723E-02
19	0.6770662E-06	0.6219309E-02
20	0.1044794E-05	0.7015895E-02
21	0.1056458E-05	0.6930754E-02
22	0.1549677E-05	0.7920235E-02
23	0.1536388E-05	0.7077474E-02
24	0.1566114E-05	0.7118322E-02
25	0.2455525E-05	0.8344624E-02
26	0.4096675E-05	0.9103846E-02
27	0.5275292E-05	0.9693377E-02
28	0.5376332E-05	0.9120602E-02
29	0.6777630E-05	0.1033259E-01
30	0.6840547E-05	0.9702038E-02
31	0.8352243E-05	0.9966750E-02
32	0.1101932E-04	0.1031952E-01
33	0.1310863E-04	0.1110057E-01
34	0.1571359E-04	0.1181628E-01
35	0.1573845E-04	0.1298212E-01

A LEAST-SQUARES FIT OF THE ABOVE DATA IS GIVEN BY :

$$K*SC^{**}(2/3) = 0.1349120E\ 00\ (ELM*VIS/DEN)^{0.219}$$

RUN	KO	SH/SC**(1/3)
17	0.4821373E 10	0.4104527E 02
18	0.2640648E 10	0.5245493E 02
19	0.5448458E 10	0.5890639E 02
20	0.8332468E 10	0.6630229E 02
21	0.8276058E 10	0.6520535E 02
22	0.1213983E 11	0.7451450E 02
23	0.1214377E 11	0.6673459E 02
24	0.1173601E 11	0.6623106E 02
25	0.1823947E 11	0.7746996E 02
26	0.3042986E 11	0.8451843E 02
27	0.3953151E 11	0.9019017E 02
28	0.3724173E 11	0.8320877E 02
29	0.5169614E 11	0.9656371E 02
30	0.5171608E 11	0.9047040E 02
31	0.6721186E 11	0.9440047E 02
32	0.8257562E 11	0.9601595E 02
33	0.9910419E 11	0.1035116E 03
34	0.1209236E 12	0.1106749E 03
35	0.1179394E 12	0.1207896E 03

A LEAST-SQUARES FIT OF THE ABOVE DATA IS GIVEN BY :

$$SH/SC^{**}(1/3) = 0.4127838E\ 00 \times KO^{0.220}$$

RUN	REM	E*SHM/SC**(1/3)
1	0.1594329E 02	0.6586272E 00
2	0.1625447E 02	0.6916112E 00
3	0.1672415E 02	0.7789844E 00
4	0.1675784E 02	0.7368323E 00
5	0.1750914E 02	0.7965418E 00
6	0.1780214E 02	0.7364063E 00
7	0.2679050E 02	0.1022712E 01
8	0.2764455E 02	0.1010583E 01
9	0.2853424E 02	0.1038817E 01
10	0.2829330E 02	0.1275385E 01
11	0.3022383E 02	0.1150296E 01
12	0.3000546E 02	0.1243452E 01
13	0.5370792E 02	0.1777454E 01
14	0.5373926E 02	0.1781634E 01

A LEAST-SQUARES FIT OF THE ABOVE DATA IS GIVEN BY :

$$E*SHM/SC**(1/3) = 0.8192831E-01 \; REM^{0.777}$$

RUN	REM	E*SHM/SC**(1/3)
13	0.5370792E 02	0.1777454E 01
14	0.5373926E 02	0.1781634E 01
15	0.6344011E 02	0.2446797E 01
16	0.6987749E 02	0.2915578E 01
17	0.7627467E 02	0.3200363E 01
18	0.9699203E 02	0.4287695E 01

A LEAST-SQUARES FIT OF THE ABOVE DATA IS GIVEN BY :

$$E*SHM/SC**(1/3) = 0.4373286E-02 \quad REM^{1.517}$$

RUN	REM	E*SHM/SC**(1/3)
18	0.9699203E 02	0.4287695E 01
19	0.1156180E 03	0.4685156E 01
20	0.1269593E 03	0.5267820E 01
21	0.1272398E 03	0.5059072E 01
22	0.1412568E 03	0.5926167E 01
23	0.1406690E 03	0.5470434E 01
24	0.1396404E 03	0.5329134E 01
25	0.2025969E 03	0.6188278E 01
26	0.2453390E 03	0.6782609E 01
27	0.2736497E 03	0.7103333E 01
28	0.2682004E 03	0.6648878E 01
29	0.3067693E 03	0.7943011E 01
30	0.3082573E 03	0.7047701E 01
31	0.3406235E 03	0.7505346E 01
32	0.4029414E 03	0.7518161E 01
33	0.4428523E 03	0.8253385E 01
34	0.4971951E 03	0.9237033E 01
35	0.4914485E 03	0.9693375E 01

A LEAST-SQUARES FIT OF THE ABOVE DATA IS GIVEN BY :

$$E*SHM/SC**(1/3) = 0.6794912E\ 00 \quad REM^{0.416}$$

APPENDIX IV

A Sample Calculation of Liquid Holdup for Run 8

Operation Conditions:

Flow regime: poor interaction regime

Temperature, °C,	: 25
Liquid flow rate, L, $kg/m^2.s$,	: 4.26
Liquid density, ρ_L, kg/m^3,	: 996.9
Liquid viscosity, μ_L, kg/m.s,	: $8.94*10^{-4}$
Pressure drop, ΔP_{LG}, N/m^3,	: 2840
Particle external surface area, a_S, m^{-1},	: 899
Particle diameter, D_P,m,	: $6.35*10^{-3}$
Porosity of bed, ε,	: 0.624

a. for dynamic holdup:

$$Re_L = \text{liquid Reynolds number} = \frac{L.D_P}{\mu_L} = \frac{4.26*6.35*10^{-3}}{8.94*10^{-4}}$$

$$= 30.27$$

$$Ga^* = \text{modified Galileo number} = \frac{D_P^3.\rho_L(\rho_L.g+\Delta P_{LG})}{\mu_L^2}$$

$$= \frac{(6.35*10^{-3})^3*996.9*(996.9*9.8+2840)}{(8.94*10^{-4})^2}$$

$$= 4.03*10^6$$

Substituting into Equation 9:

$$\beta_D = 3.86\ (Re_L)^{0.545}\ (Ga^*)^{-0.42}\ \left(\frac{a_S.D_P}{\varepsilon}\right)^{0.65}$$

$$= 3.86\ (30.27)^{0.545}\ (4.03*10^6)^{-0.42}\ \left(\frac{899*6.35*10^{-3}}{0.624}\right)^{0.65}$$

β_D = 0.175

h_{LD} = $\varepsilon.\beta_D$ = 0.624*0.175 = 0.1094

b. for static holdup:

static holdup = $3.2*10^{-4}*(d_p)^{-1.56}$ (A)

= $3.2*10^{-4}*(0.00847/0.3048)^{-1.56}$

=0.0855

where Equation A was obtained from Shulman et al. (35).

Value of static holdup from Standish (36) is 0.0803.

Then,

average of static holdup = (0.0855+0.0803)/2

= 0.0828

total holdup = static holdup + dynamic holdup

= 0.1094 + 0.0828

= 0.192